

NORTHWESTERN UNIVERSITY

Network Failure, Atrophy, and Tau Pathology in Aphasic Alzheimer Disease

A DISSERTATION

SUBMITTED TO THE GRADUATE SCHOOL
IN PARTIAL FULFILLMENT OF THE REQUIREMENTS

for the degree

DOCTOR OF PHILOSOPHY

Field of Neuroscience

By

Adam Christopher Martersteck

EVANSTON, ILLINOIS

June 2020

—ABSTRACT—

Network Failure, Atrophy, and Tau Pathology in Aphasic Alzheimer Disease

Adam Christopher Martersteck

Brain network organization, the emergence of cognition, and the accumulation of neurodegenerative pathology are interwoven concepts frequently studied under the umbrella of behavioral neurology, neuropsychiatry, neuropsychology, and neuropathology. One approach to studying the organization of cognitive processes is to study individuals with selective deficits. To understand how a system fails and deficits arise, it is critical to understand its structural and physiologic underpinnings. To study the origin and spread of disease, understanding the routes of functional and structural communication between the brain is essential. The two studies presented in this dissertation are based on such a model. Using neuroimaging in human participants, we studied differences in functional networks, atrophy, cognition, and accumulated AD pathologic burden.

Study 1 examined differences between phenotypes of Alzheimer disease (AD) using network measure from resting state fMRI. Our models for studying differences in brain network integrity were, (1) participants with amnesic dementia, with primary deficits in episodic memory, and (2) participants with primary progressive aphasia (PPA), characterized by the loss of language. Both patient groups showed biomarkers consistent with or had autopsy proven AD neuropathology.

We tested the hypothesis that although both groups had the same cellular neuropathology, characterized by an abnormal aggregation of amyloid- β and hyperphosphorylated tau, they would show differential network disruption, which is more closely aligned with their clinical phenotype. Namely, the amnesic dementia group would have deficits in an large-scale network for episodic memory, while the PPA group would have deficits in a left-lateralized language network.

Furthermore, we hypothesized that both dementia syndromes would have lower network connectivity of a different large-scale network, the default mode network (DMN), which has previously been shown to be vulnerable across a wide range of disconnection syndromes and may not be specific for a single clinical disorder. Consistent with our hypotheses, we found (1) the PPA group had less functional connectivity of the language network compared to amnesic dementia group, (2) amnesic dementia participants had less connectivity of the episodic memory network, and (3) both syndromes showed reduce connectivity within the DMN.

Study 2 focused exclusively on PPA with suspected underlying AD to study the relationship between cognition, structural atrophy, and AD tau pathologic burden measured by positron emission tomography. We tested our hypotheses with a measure of object-naming, which we hypothesized would show a more focal relationship with atrophy and more widespread relationship among connected networks for tau pathology. But in examining or predicting the future decline in naming, that tau pathology would be the leading indicator. Furthermore, we hypothesized that tau and atrophy would have a strong association throughout the brain. Consistent with prior observations from our lab and others, naming was associated with the left-lateralized language network tau and atrophy. The significant relationship between tau and naming showed a more widespread pattern than the association between naming and atrophy. Consistent with network models of naming, left anterior temporal lobe tau burden was the only predictor of future decline. We found a strong overlap with tau and atrophy, which was enhanced once we accounted for age.

Overall, these studies used cutting edge methodology and materials in a unique patient population to test hypotheses related to large-scale networks, cognition, and accumulating AD pathology. Results from the studies have implications for the selective vulnerability of networks, the spatial distribution of clinicopathologic correlations, and relationships between tau pathology and neurodegeneration, further clarifying the neurobiology of neurodegenerative syndromes.

—TABLE OF CONTENTS—

ABSTRACT.....	3
GENERAL INTRODUCTION.....	7
Tomographic imaging.....	11
Measuring brain atrophy <i>in vivo</i>	13
Exploring large-scale brain networks.....	15
STUDY 1: DIFFERENTIAL NEUROCOGNITIVE NETWORK PERTURBATION IN AMNESTIC AND APHASIC ALZHEIMER DISEASE.....	20
Introduction.....	22
Methods.....	22
Results.....	25
Discussion.....	29
STUDY 2: TAU BURDEN, ATROPHY, AND NAMING IN THE APHASIC VARIANT OF ALZHEIMER DISEASE.....	31
Introduction.....	33
Methods.....	35
Results.....	43
Discussion.....	53
GENERAL CONCLUSIONS.....	59
REFERENCES.....	65

—LIST OF TABLES & FIGURES—

STUDY 1

Table 1.1 Demographic and neuropsychological performance of primary progressive aphasia, dementia of the Alzheimer type, and normal control participants.....26

Figure 1.1 Resting-state connectivity differences between primary progressive aphasia with suspected underlying Alzheimer disease compared to dementia of the Alzheimer type.....28

Figure 1.2 Resting-state connectivity differences from the default mode network between primary progressive aphasia with suspected underlying Alzheimer disease and dementia of the Alzheimer type groups compared to normal controls.....29

STUDY 2

Table 2.1 Demographic and neuropsychological performance of primary progressive aphasia participants.....44

Figure 2.1 PPA-AD group patterns of tau PET and MRI atrophy.....46

Figure 2.2 Association of tau burden on cortical thickness and age.....47

Figure 2.3 Association between baseline BNT with cortical thickness and tau burden.....48

Figure 2.4 Regional analyses confirm surface-wise findings for associations between BNT, thickness, and tau.....49

Figure 2.5 Atrophy and tau burden share and uniquely explain scores on the BNT while tau alone shows non-linear relationship.....51

Figure 2.6 Left hemisphere anterior temporal tau is associated with future decline in naming.....52

—GENERAL INTRODUCTION—

Alzheimer disease (AD) was first described in 1906 by a German psychiatrist and neuropathologist named Alois Alzheimer (**Alzheimer, 1906**). He had followed the 5-year progression of a woman who presented with rapid memory loss, disorientation, and paranoia, but preserved motor coordination and reflexes. At autopsy, the 56-year old woman had general cortical atrophy. Using the newly developed Bielschowsky silver stain, Alzheimer noted tangles of neurofibrils in ~30% of all the cells examined. He further reported the millet seed-like deposition of a peculiar substance throughout the cortex. These two observations would go on to form the basis for the pathological diagnosis of AD: the presence of neurofibrillary tangles (NFTs) and amyloid- β (A β) plaques. Alzheimer's and his contemporaries had initially defined it as a clinicopathologic entity, the NFTs and A β plaques caused a rare syndrome called presenile dementia that occurred before old age (**Kraepelin, 1910**). It would be several decades before research transformed our understanding of AD by finding a strong correlation between senile dementia and AD pathology in elderly nursing home patients (**Blessed, et al., 1968**).

A consensus was reached for the clinical diagnosis of AD in 1984 (**McKhann, et al., 1984**). It was again defined as a joint clinicopathologic entity, diagnosed in life as “possible AD” or “probable AD”, then confirmed as “definite AD” at autopsy. As a consequence, the term AD is frequently used to describe two separate but related entities: (1) AD neuropathologic change (ADNC), the presence of NFTs and A β plaques made at autopsy (**Hyman, et al., 2012; Montine, et al., 2012a**); (2) the clinical syndrome, usually amnesic, suspected to be caused by ADNC. Although the diagnostic criteria have been updated (**McKhann, et al., 2011**), the shared nomenclature and blurring between pathologic entity and clinical syndrome continues to cause confusion and disagreements about usage of the term AD (**Jagust, et al., 2019; Jack, 2020**). Throughout this dissertation, I will use the term AD to refer strictly to the underlying

neuropathologic change and the term dementia of the Alzheimer type (DAT) to refer to the clinical syndrome.

Since the original formulation of the AD clinical and pathologic diagnoses, several “atypical” variants of AD have been described, including primary progressive aphasia (PPA) (**Mesulam, 1982; 2003**), posterior cortical atrophy (PCA) (**Benson, et al., 1988; Hof, et al., 1989; Hof, et al., 1993; Crutch, et al., 2017**), and a primarily behavioral/executive frontal-type AD (**Johnson, et al., 1999; Ossenkoppele, et al., 2015b**). Atypical because the primary domain of cognition most affected is non-memory but the causative underlying pathology is the same hallmark NFTs and A β plaques. The atrophy and Braak NFT staging patterns (**Braak, et al., 1993; Braak and Del Tredici, 2011; Braak, et al., 2011**) violate the “typical AD” pattern of entorhinal-first and instead follow a clinically concordant pattern with higher densities of NFTs found in frontal regions (frontal AD), left hemisphere language regions (PPA), or posterior visuospatial regions (PCA) (**Murray, et al., 2011; Gefen, et al., 2012; Mesulam, et al., 2014; Ossenkoppele, et al., 2015a; Ohm, et al., 2020**).

PPA is a progressive dementia syndrome characterized by the primary dissolution of language while memory and other cognitive functions remain initially preserved (**Mesulam, 1982; 2003**). The most common neuropathologic correlates are AD (~40%) or a form of frontotemporal lobar degeneration (FTLD; ~60%), with either abnormally phosphorylated tau (FTLD-tau) or TAR DNA binding protein 43 kDa (FTLD-TDP43) type pathology (**Mesulam, et al., 2014**). PPA with underlying AD pathology (PPA-AD) is the aphasic variant of AD (**Rogalski, et al., 2016**). Several clinical variants of PPA are described that subtype patients by the specific subdomains of language most affected (**Mesulam, et al., 2009; Gorno-Tempini, et al., 2011**). The three recognized research subtypes of PPA are logopenic (PPA-L), agrammatic (PPA-G), and semantic (PPA-S). While there are strong relationships between spatially localized cortical atrophy and specific language deficits (**Rogalski, et al., 2011a; Mesulam, et al., 2015; Mesulam, et al., 2019**)

or subtypes (Rohrer, *et al.*, 2009; Rogalski, *et al.*, 2011b; Ridgway, *et al.*, 2012), the relationship is probabilistic between subtypes and underlying pathology (Mesulam, *et al.*, 2014).

Neuroimaging modalities have been used in the field of neurology since their inception. Medical imaging has frequently been used for the exclusion of other causative factors to explain the loss of cognition (e.g. infarcts or lesions). More recently, *in vivo* imaging is being used alongside neuropsychological tests to assess a patient's brain integrity or probable pathology as outcome measures in clinical trials (Sperling, *et al.*, 2014). For observational and interventional research, the recent National Institute on Aging and Alzheimer's Association (NIA-AA) criteria have further complicated the diagnoses (for research) by suggesting that ADNC can be classified during life, by operationalizing CSF and/or imaging biomarkers of amyloid and tau (Jack, *et al.*, 2018). The amyloid, tau, and neurodegeneration A/T/(N) staging scheme seeks to create a biomarker-based definition of AD. Like previous classifications of AD, it has been met with criticism and misunderstanding (Frisoni, *et al.*, 2019; Jagust, *et al.*, 2019; Sweeney, *et al.*, 2019; Jack, 2020).

Thresholds for what constitutes sufficient amyloid, tau, or neurodegeneration (A+/T+/N+ vs. A-/T-/N-) are still being defined (Jack, *et al.*, 2015; Jack, *et al.*, 2016a; Jack, *et al.*, 2016b). Of the thresholds that have been established, amyloid PET thresholds have used short interval imaging-to-autopsy correlations that include pathology from sporadic late-onset amnesic dementia patients and elderly participants without cognitive decline (Ikonomovic, *et al.*, 2008; Clark, *et al.*, 2011; Clark, *et al.*, 2012; Joshi, *et al.*, 2012; Sabri, *et al.*, 2015; Seo, *et al.*, 2017). They have found greater than 90% sensitivity and specificity in participants with *in vivo* amyloid PET and subsequent post-mortem measured plaque burden (Klunk, *et al.*, 2004; Barthel, *et al.*, 2011; Clark, *et al.*, 2011; Irwin, *et al.*, 2012). Measures of neurodegeneration have typically come from large cohort studies examining CSF total tau, FDG PET hypometabolism, or MRI structural atrophy patterns (Jack, *et al.*, 2015; Jack, 2016). The biomarker for the NFT burden,

the “T” in the A/T/(N) model, can be defined by CSF phospho-tau or by tau PET, the most recent imaging biomarker to be added to the AD researchers repertoire. To date, tau PET thresholds are beginning to be defined based on typical AD Braak NFT stages (**Maass, et al., 2017**). Atypical forms of AD like PPA do not have alternate imaging biomarker definitions (i.e. sampled from different regions of the brain) to match the differing spatial patterns of atrophy (**Rogalski, et al., 2011b; Rogalski, et al., 2014**), NFT burden (**Gefen, et al., 2012**), and possibly amyloid (**Martersteck, et al., 2016**) compared to typical AD.

Medical neuroimaging research has typically been used for two broad categories: (1) with the goal of providing new information for the identification/treatment of neurologic syndromes or underlying brain pathology or (2) comparing patient groups that deviate from normal to study the neural correlates of behavior or understand the neurobiology of the brain during disease. This dissertation is primarily focused on (2), with the hope that the research done here will be used to develop tools for inclusion of under-represented phenotypes such as PPA-AD into clinical trials or for the identification of markers that may predict individualized clinical progression.

The focus of this dissertation will be on exploring the relationship between functional brain networks in PPA-AD compared to DAT (Experiment 1) and the multi-modal relationships between atrophy, tau pathology, and cognition in PPA-AD (Experiment 2). Given the small sample sizes available in studies of atypical dementia like PPA-AD, the research pays particular importance to using the best available neuroimaging hardware, materials, and methods to increase statistical power and our ability to detect differences.

The following sections provide a brief overview of history and the modalities that were used to probe relationships in the brain and how they have been used in prior research in AD.

Tomographic imaging

The three main tomographic imaging techniques, CT, MRI, and PET were all developed in parallel in the late 1970s and early 1980s. Computed tomography (CT) scanners were first designed and constructed by Godfrey Hounsfield in 1967, the first brain scan performed in 1971, and full-body scanner built in 1975. By 1980, three million CT scans had been performed and Hounsfield and Cormack had won a Nobel Prize. A CT scanner is made up of a patient table or bed and a gantry that holds a ring with an X-ray tube, filter, and collimator on one end, and a detector array on the opposite end. As the gantry spins, the X-ray tube cathode accelerates electrons with a high voltage. The sudden deceleration as the electrons collide with the anode generates X-rays. The X-ray beams pass through a layer of biological material and strike the detectors on the opposite end. The amount that the X-ray is attenuated (i.e. photons are absorbed) as it passes through material is in direct relation to the electron density of the tissue. For example, bones absorb more photons than water or fat and thereby have different Hounsfield units on the reconstructed CT. By taking measurements of the X-ray from many different angles (i.e. slices) as the gantry rotates, we can add depth and a third dimension.

Edward Mills Purcell and Felix Bloch had first described Nuclear Magnetic Resonance (NMR) in 1946. At the same time that Hounsfield was developing the first CT near London, UK, Paul Lauterbur at Stony Brook University had discovered the possibility of creating a 2D image by using varying magnetic gradients in a strong magnetic field (**Lauterbur, 1973**). Peter Mansfield expanded on Lauterbur's work at the University of Nottingham. Mansfield realized we could formulate spin physics in a Fourier 'k-space', replacing the projection reconstruction method with frequency and phase encoding spatial gradients, allowing scans take seconds instead of hours. Lauterbur and Mansfield would share the Nobel Prize in 2003 for their discoveries that led to MRI.

While NMR was being discovered and the first CT and MRI were being invented, several teams of researchers from Massachusetts General Hospital (MGH), Brookhaven National Lab,

and University of California Berkeley were laying the foundation for PET. They were trying to localize brain tumors by using sodium iodide detectors to detect the coincidence events of 511-keV photons produced during annihilation radiation [6, 7, 8]. The first 2D array, called a positron camera, was developed in the early 1970s, and used photomultipliers to enhance the very weak single photon signals [10]. Inspired by Hounsfield's CT system, researchers from MGH and Washington University in St. Louis, including Ter-Pogossian, Phelps, and Hoffman built the first PET scanner, with a hexagonal array of scintillation detectors protected by shielding, for the reconstruction of a tomographic image (**Phelps, et al., 1975; Ter-Pogossian, et al., 1975**).

PET leverages the above technology jointly with our ability to create radioactive tracers that have specific molecular targets. We can then estimate and visualize physiology or pathology that are indiscernible on CT or MRI. For example, the most popular PET ligand, ^{18}F -fluorodeoxyglucose (FDG), is a glucose analog taken up by high-glucose using cells throughout the body. But because FDG has substituted the 2-hydroxyl group necessary for glycolysis for the radioactive fluorine-18, it cannot be metabolized by cells after uptake. We can then visualize the amount of FDG that is taken up all over the brain based on the underlying physics of positron annihilation. As the unstable radionuclide sits in the cell, it decays, interacting with an electron and producing anti-parallel gamma rays that strike scintillation crystals on opposite sides of the PET detector ring. Based on hundreds of thousands of annihilation events, recorded by the PET scanner with picosecond resolution, we can reconstruct estimates of where in the brain FDG is concentrated.

The development of radiotracers that bind pathology has been a major goal of medical neuroimaging. Early PET studies mainly focused on basic brain human physiology. Studies utilized oxygen-, carbon-, or fluorine-labelled PET tracers to examine regional blood flow (**Ter-Pogossian, et al., 1969**), glucose utilization (**Raichle, et al., 1975**), cerebral blood volume (**Eichling, et al., 1975**), or vascular permeability (**Raichle, et al., 1976**). FDG PET has been a

mainstay of research and clinical use for oncology and neurodegenerative disease since the '80s. But a major goal of PET imaging has been the ability to quantify pathology *in vivo*, such as the hallmark proteins of AD, NFTs and A β plaques. In 2004, a major breakthrough was made when a carbon-labelled tracer, Pittsburgh Compound B, was developed to quantify A β (Klunk, *et al.*, 2004). Unfortunately, creating a fluorine-labelled amyloid tracer would take several more years. Around 2010, a slew of ^{18}F -labelled amyloid tracers were developed in short succession, including florbetapir (Choi, *et al.*, 2009; Wong, *et al.*, 2010), florbetaben (Villemagne, *et al.*, 2011), flutemetamol (Nelissen, *et al.*, 2009; Vandenberghe, *et al.*, 2010), and NAV4694 (Jureus, *et al.*, 2010; Rowe, *et al.*, 2013). The first generation tau tracer, ^{18}F T807, later called AV-1451, now called flortaucipir, would follow shortly after (Chien, *et al.*, 2013; Xia, *et al.*, 2013). Second generation tau tracers such as RO-948, MK-6240, THK-5351, THK-5317, PI-2620, APN-1607, and PBB3 all still must undergo the critical validation steps the first generation tau and amyloid tracers have gone through. This dissertation will focus on using the amyloid PET tracers florbetapir and florbetaben to determine "amyloid positivity" among participants. The first generation tau tracer flortaucipir will play a major role in Study 2.

Measuring brain atrophy *in vivo*

Alzheimer described his 56-year old patient as having 'general cortical atrophy' upon examination of her brain. What he was referring to was a shrinking of the outer layer of the brain, observable with the human eye. Cortical grey matter is everything from the neuropil, the dendrites and unmyelinated axons, to glial cells, including astrocytes and oligodendrocytes, to the neural cell bodies. It is made up of synapses from one cell to another and the capillaries that route blood between arterioles and venules. Reductions in synapses or in dendric arborization, neuronal or glia cell shrinkage or cell death all cause a reduction in grey matter. Technically, hydration will

also influence the thickness of grey matter, but dehydration is not considered tissue loss or atrophy.

We can measure the thickness or volume of grey matter with high-resolution structural CT or MRI image. As opposed to functional imaging, described above, structural imaging typically provides static anatomical information. Here, we will talk about the use of T₁- and T₂-weighted MRI scans. These single 3D images have high signal-to-noise and high contrast, and are able to differentiate between brain tissue compartments. Modern scans typically take between 4-10 minutes to acquire a whole brain volume at spatial resolutions between 0.7 mm³ to 1 mm³. They are highly sensitive to motion, as they are analogous to taking a single long exposure photograph.

The first studies examining AD with MRI found diagnostic value and neuropsychological correlates (**Seab, et al., 1988; Jack, et al., 1989; Press, et al., 1989; Kesslak, et al., 1991; Scheltens, et al., 1992**). Specifically, they found the contrast superior to CT and found clinicoanatomic correlates between the hippocampus and surrounding structures with global and memory-specific cognitive measures. Scans were typically ranked by radiologists as quantitative scores between 0-4. Since the late '80s, computers have improved dramatically and now allow algorithms to characterize the morphology of the brain. One of the first methods invented was called the boundary shift integral (**Freeborough and Fox, 1997**) and it was first used for looking at progression of atrophy in amnesic AD (**Fox and Freeborough, 1997**). It examined the differences in grey matter boundaries based on how grey matter voxel intensities differed between scans.

More than two decades of development later, the popular structural neuroimaging software suites typically involve more than 25 different processing stages, beyond the scope of this dissertation. The method used within this dissertation generates reconstructions of the inner and outer surface of the brain. The inner surface, at the junction of white matter and grey matter, is called the "white surface" and is analogous to where the growth rings of a tree meet the bark.

The outer surface, at the junction of the where the outer grey matter meets the CSF/skull is analogous to the outer part of the tree's bark. Cortical thickness, and its counterpart cortical thinning or atrophy, is calculated as the distance between both the inner and outer surfaces.

Exploring large-scale brain networks

Mesulam said, "Networks provide the scaffolding for the computational architectures that mediate cognitive functions" (**Mesulam, 2009**). Cognition does not exist at the level of proteins, synapses, or cells. Cognitive neuroscience has struggled with a model for the neural substrates of cognition since Wernicke, Lichtheim, Charcot, James, Jackson, and Freud in the late 1800s. And in the 1950s and '60s by McCulloch, Pitts, Hebb, Lashley, and Geschwind. As technology advanced in the '80s, analogies could start to be made between the brain and computer. One of the most influential movements in modern cognitive neuroscience emerged when McClelland and Rumelhart published *Parallel Distributed Processing* and asked, "What makes people smarter than machines?" (**Rumelhart and McClelland, 1986**). Cognitive neuroscientists argued between theories. One, a theory of a central executive that controlled the functional integration of information through linear hierarchical processing, organized from the bottom up. The second, organized as decentralized parallel processing with recurrent and recursive neural interactions (**Edelman, 1978; 1987**), such as parallel streams of information for color or motion in visual processing (**Felleman and Van Essen, 1991**).

Mesulam proposed that brain-behavior relationships were both localized and distributed (**Mesulam, 1990**). That cognition arose from a 'multifocal neural system' instead of from local regional processing. In Mesulam (**1998**), he expanded the theory by envisioning the brain as arranged along a 'core synaptic hierarchy' that consisted of primary sensory, modality-selective, heteromodal, paralimbic, and limbic zones. That downstream transmodal areas (the latter three along the hierarchy) are nodes of convergence that act to integrate and bind modality-specific

upstream signals into multimodal representations. Instead of individual neurons coding complex percepts, it is the relative firing frequencies within these downstream neurocognitive networks. This graded signal allows for far more coded features with the same number of parts. He emphasized that the cooperative processes of nodes are shaped by anatomical connectivity. Thus, cognition arises as a collective property out of parallel distributed processing units interconnected in complex configurations influenced by anatomical connectivity.

Definitions of what constitutes a network vary depending on scale. For example, local networks of neurons may operate within a single cortical region, such as the linking of receptive fields in visual cortex (**Lehky and Sejnowski, 1988**) or inter-laminar integration of cortical minicolumns (**Opris, et al., 2017**). The network systems described herein are of the large-scale hub-and-spoke variety and are spatially distributed throughout the brain. At the most basic level, the large-scale networks can be partitioned into two divisions: upstream sensory and downstream association. Mesulam (**1990; 1998**) gave evidence for five large-scale discrete systems: a frontoparietal spatial attention network, a left hemisphere perisylvian temporal language network, an explicit memory and motivation limbic network, an inferotemporal face and object recognition network, and prefrontal executive function network. For further review, see (**Mesulam, 2008**).

Using neuroimaging is one way of studying brain networks. One popular modality is called resting state functional MRI (fMRI). Due to the spatial limitations of neuroimaging (on the millimeter scale), network solutions for the human brain typically involve between 50-1,000 nodes and 5-20 distributed networks. An example partition would be the network solutions by Yeo and colleagues (**Yeo, et al., 2011**). They partitioned the entire brain resting state fMRI into 1,175 4mm² patches across the cortical surface and ran a clustering algorithm on 500 participants. They examined confidence of the clustering solution in a hold-out validation group of 500 different participants. They found the highest stability for discrete networks was 7, 10, 12, and 17 different communities of networks. A separate group of researchers, part of the Human Connectome

Project, found 360 cortical regions per brain best represented the functional connectivity and structural topography of 210 healthy young adults (**Glasser, et al., 2016**). Iterative Louvain clustering divided the 360 regions into 12 networks: orbito-affective, default mode, auditory, frontoparietal, language, dorsal attention, cingulo-opercular, somatomotor, secondary visual, primary visual, ventral and posterior multimodal (**Ji, et al., 2019**).

Functional MRI works by exploiting several key properties of physics and brain physiology. Especially important for cognitive neuroscience and brain mapping, is the concept of neural coupling. That hemodynamics throughout the brain are coupled to neural activity through oxidative metabolism and energy demand. For a review see (**Fox, 2012**). Research using simultaneous fluorodeoxyglucose (FDG) PET and fMRI has shown a strong association between the local neural metabolism and the changes we observe with fMRI (**Riedl, et al., 2014; Savio, et al., 2017**). We can observe these changes with MRI using a T_2^* -weighted contrast called the blood oxygen level dependent (BOLD) signal. It leverages the fact that when hemoglobin becomes deoxygenated it gains a paramagnetic charge (**Pauling and Coryell, 1936**). The difference in local susceptibility between the blood vessel and surrounding tissue creates a measurable distortion in the magnetic field. Based on the response rate of the local vascular network, the time lag between neural activity, vasodilation, and increased blood flow all leads to observable fMRI signals on the order of 10s of seconds (e.g. 0.01-0.001 Hz), first observed in resting state studies in (**Biswal, et al., 1995**).

The name resting state fMRI (rs-fMRI) is a bit of a misnomer. Prior the advent of rs-fMRI, researchers typically had a participant laying in the scanner instructed to perform an active task, such as differentiating between an on-screen picture of a house or a face. While the same T_2^* -weighted BOLD contrast is collected, the instructions changed from an outward task to asking the participant to simply remain still, typically with their eyes open. But the participant continues to be engaged in internally directed processes, such as recollecting past events or planning for future

ones. The brain's organization (i.e. clustering solution, as described above) does not change dramatically during an externally directed task compared to "rest". Electroencephalography (EEG) patterns during resting states exhibit structured activity patterns that reflect ongoing mental activity (**Berger, 1931b; a**). An analysis of participants with paired resting state and task-based fMRI found the same network properties and amplitudes of signal irrespective of if the participant was in the task state or resting state (**Smith, et al., 2009**). Therefore, it may be more appropriate to call it "task free state" instead of "resting state".

Networks of regions all over the brain continue to spontaneously oscillate, activating and deactivating in synchrony, during the task free time in the scanner. Like playing a video of the 3D brain volumes, we can analyze this synchronous neural activity over the course of a typical 5 to 15 minute scan to generate patterns of network activity. A statistic, functional connectivity, describes the temporal coherence in the BOLD timeseries between two or more regions. After we have calculated the paired node-to-node functional connectivity we can define a network. Simply, a network is two or more regions wherein nodes show stronger functional connectivity (temporal coherence) within a group than outside the group. Several different mathematical methods, outside the scope of this work, are employed to determine the community structure of a network. Early studies demonstrated that we could find and identify the type of large-scale spatially distributed networks described by Mesulam in 1990 with rs-fMRI (**De Luca, et al., 2006**).

The first studies examining resting state fMRI networks in AD (**Lustig, et al., 2003; Greicius, et al., 2004**) found differences from cognitively normal controls in a network called the 'default mode network' (DMN) (**Raichle, et al., 2001**). The DMN is most commonly described as comprising of retrosplenial, parahippocampal, medial prefrontal, posterior inferior parietal lobule, temporoparietal junction, lateral temporal, temporal pole, and hippocampal formation. Like most networks, it can be partitioned into successively smaller clusters. Andrews-Hanna and colleagues (**Andrews-Hanna, et al., 2010b**) describe the DMN as comprising of three subsystems, a "core"

along the medial frontal and posterior cingulate with branches to a medial temporal lobe subsystem and a dorsal medial prefrontal cortex subsystem.

The DMN is preferentially active when individuals are in a task free state and not focused on external environmental cues. The network is thought to act as a mental simulator. It supports cognitive systems for internal autobiographical memory retrieval, envisioning of the future, and taking the perspective of others (**Buckner, et al., 2008; Andrews-Hanna, et al., 2010a**). The (phylogenetically) recent hominin evolution and areal expansion of association cortex (**Buckner and Krienen, 2013**) may play a role in human's unique ability to simulate and predict the consequences of events we've never experienced (**Gilbert and Wilson, 2007**). It is thought the neural network responsible for such ability resides within the DMN. Because the DMN is preferentially active during task free periods and is linked to large cortical regions (which may make it methodologically easier to analyze them), it is frequently studied with rs-fMRI. The finding that it is functionally less connected is not specific to AD, as several conditions are associated with a reduced DMN activity, including autism, depression, epilepsy, schizophrenia, and related dementia syndromes. For a review of implicated 'disconnection syndromes' see (**van den Heuvel and Sporns, 2019**).

—STUDY 1—

**Differential Neurocognitive Network Perturbation in
Amnesic and Aphasic Alzheimer disease**

Objective

To determine if resting state fMRI connectivity (rs-fMRI) patterns differentiated the amnesic from aphasic phenotypes of Alzheimer disease.

Methods

Three groups were investigated: 14 participants suspected of having the neuropathology of Alzheimer disease (AD) based on clinically diagnosed amnesic dementia of the Alzheimer type (DAT), 26 individuals with primary progressive aphasia (PPA) with either a positive ¹⁸F-florbetapir amyloid PET scan and/or confirmed AD at autopsy, and 26 neurologically intact controls. The groups were compared using rs-fMRI. Seeds included the left hemisphere inferior frontal gyrus (IFG) for the language network, the left hippocampus for the episodic memory network, and the left posterior cingulate for the default mode network (DMN).

Results

Greater connectivity perturbations were found from the hippocampus for the DAT group, and from the IFG for the PPA group. Furthermore, connectivity alterations in the PPA group were more asymmetric and favored the language dominant left hemisphere. Loss of connectivity from the DMN seed was of a similar magnitude in the PPA and DAT groups.

Conclusions

Despite the presumptive common underlying neuropathology of amyloid plaques and neurofibrillary tangles, the two groups displayed two different patterns of network perturbation, each concordant with the clinical presentation and the anatomy of neurodegeneration.

INTRODUCTION

In typical sporadic late-onset Alzheimer disease (AD), the core amnesic deficit arises due to an accumulation of pathology and atrophy of the medial temporal cortex, an episodic memory network hub. One atypical phenotype of AD, primary progressive aphasia (PPA), is characterized by language impairment with predominant accumulation of neuropathology and atrophy in the left hemisphere perisylvian language network (**Gefen, et al., 2012; Rogalski, et al., 2016**). PPA-AD patients have the same characteristic neurofibrillary tangles and amyloid-beta ($A\beta$) plaques as those with amnesic-AD (DAT), albeit with a different spatial distribution (**Gefen, et al., 2012**).

Selective vulnerability for the language network in PPA-AD and of the medial temporal memory network in DAT-AD has been well characterized by atrophy and FDG PET hypometabolism (**Jack, et al., 2013**). However, less is known about how the disruption of large-scale distributed networks that support cognition differ by AD phenotype. This study used resting state fMRI (rs-fMRI) to examine network level differences between aphasic versus amnesic AD phenotypes in three networks: the language network, episodic memory network, and default mode network (DMN). We hypothesized differences would be clinically concordant, with reduced connectivity of the language network in PPA-AD, reduced connectivity of the episodic memory network in DAT, and no DMN connectivity differences between PPA-AD and DAT because the DMN has no known domain-specific functional affiliation.

METHODS

Participants.

Twenty-seven individuals with a root diagnosis of PPA enrolled in Northwestern's PPA research program were identified based on 1) a T_1 -weighted structural and resting state fMRI scan, 2) positive ^{18}F -florbetapir amyloid PET, and/or 3) AD at autopsy. Fifteen individuals with a clinical diagnosis of DAT and 26 normal controls (NC) of a similar age and education with identical

MRI scans were included as comparison groups. NC participants were screened prior to enrollment for major medical conditions. The PPA and DAT participants were diagnosed by a neurologist based on clinical judgement and neuropsychological testing using previously described criteria (McKhann, *et al.*, 2011; Mesulam, *et al.*, 2012). Briefly, the PPA diagnosis was based on identification of an isolated and progressive language disorder consistent neurodegenerative etiology. T₂ FLAIR scans were used to rule out the presence of vascular lesions.

Standard protocol approvals, registrations, and patient consents.

Northwestern's Institutional Review Board approved the study. Informed consent was obtained from each participant.

MRI & resting state BOLD fMRI acquisition and analysis.

MR scanning for all participants was performed on Northwestern's 3-tesla Siemens TIM Trio. A 10-minute EPI (3.0x1.7x1.7mm³, TR=2.5sec, TE=20ms) was acquired over 11.5 minutes (244 total 3D volumes). A 1mm³ T₁-weighted 3D magnetization-prepared gradient-echo (MPRAGE) scan with 176x 1.0mm sagittal slices, an in-plane resolution of 1.0x1.0mm², TR=2300ms, TE=2.91ms, TI=900ms, and 9° flip angle was acquired and reconstructed with FreeSurfer (version 5.1.0; surfer.nmr.mgh.harvard.edu). Topological defects and inaccuracies in the estimation of the surfaces were manually corrected using FreeSurfer validated guidelines (Segonne, *et al.*, 2007).

Pre-processing of the fMRI timeseries followed standard procedure, with a few alterations for a FreeSurfer surface-based analysis. We discarded the first 4 volumes for T₁-equilibrium effects, performed rigid alignment for motion, applied slice-timing correction, bandpass filtering (0.01 to 0.1Hz), and registered the anatomical scan to the functional scan using a surface

boundary-based registration optimized for EPI-distorted sequences (**Greve and Fischl, 2009**). The principal components of motion, CSF, and eroded white matter signal were regressed as sources of spurious variance. On a per-subject basis, motion corrupted TRs were removed by calculating the frame displacement (FD) and the root mean square of the differentiated BOLD timeseries (DVARs) (**Power, et al., 2014**). A threshold of 0.3mm FD and 0.5% DVARs was used, removing the TR that violated criteria, the 1 TR before, and 2 TRs after. If a participant lost more than 30% of the timeseries (< 8 minutes of scan time remaining), they were dropped from the analysis.

Three dilated spherical surface seeds were chosen based on the areas of highest confidence in the network assignment by (**Ji, et al., 2019**) using the (**Glasser, et al., 2016**) parcels: left inferior frontal gyrus (IFG; MNI305 -50,22,16) for the language network; left hippocampus (MNI305 -25,-15,-20) for the episodic memory network; left posterior cingulate / precuneus (PCC; MNI305 -6,-50,28) for the DMN. Each seed started at approximately 200mm³ grey matter volume (equivalent to 7mm diameter sphere). The seed ROI then underwent partial volume fraction correction, which reduced the grey matter signal to approximately 50mm³ (equivalent to 4.5mm diameter sphere) of voxels that the resting state signal was averaged over. These fsaverage seeds were spherically warped to subject's native surface and projected into EPI volume space based on the surface-defined cortical ribbon and FreeSurfer's boundary-based registration from EPI to T₁. BOLD contrast effect seed-to-vertex maps were calculated regressing the top three principal components of motion, CSF, and white matter.

Statistics.

Differences in demographics and neuropsychological performance between groups were assessed with ANOVA, two-tailed independent two-sample *t*-tests, or χ^2 . For the seed-to-vertex analysis, a pseudo mixed effects analysis was performed using a weighted least squares random

effects model, taking first level subject contrast effect variance to the group level (**Roche, et al., 2007**). Cluster-wise corrections for multiple comparisons used Metropolis-Hastings Markov chain Monte Carlo simulations at a cluster-forming threshold of $p < 0.01$. The vertex-wise corrected statistical test results are displayed as clusters on FreeSurfer's template brain.

PET processing and analysis.

Amyloid PET processing followed the current ^{18}F -florbetapir standard (**Fleisher, et al., 2011**). Briefly, Statistical Parametric Mapping was used to calculate the standard uptake value ratio value (SUVR) with a florbetapir PET template and six bilateral regions: anterior and posterior cingulate, precuneus, medial orbital frontal, lateral temporal, and superior parietal (**Fleisher, et al., 2011**). A conservative mean cerebral-to-cerebellar SUVR ≥ 1.17 threshold was used for amyloid positivity (**Fleisher, et al., 2011**).

RESULTS

Of the 27 PPA participants, suspicion or confirmation of AD was determined as follows: 12 received AD neuropathologic diagnosis at autopsy (of these, 5 also had a positive amyloid PET scan), and 15 were amyloid positive on PET. Five DAT participants came to autopsy showing high AD neuropathologic change. None of the autopsied cases had co-morbid frontotemporal lobar degeneration pathology, which is consistent with previous reports (**Mesulam, et al., 2014**). One PPA-AD and one DAT participant were excluded due to excessive motion (**Power, et al., 2012**), leaving 26 PPA-AD, 14 DAT, and 26 NC for analysis. There were no significant demographic differences (**Table 1.1**; $p > 0.05$). PPA-AD and DAT participants did not differ in symptom duration or MMSE ($p > 0.05$). The PPA-AD group was significantly more impaired than the DAT group on the BNT ($p = 0.021$). MMSE ($p > 0.05$). The PPA group was significantly more impaired than the DAT group on the BNT ($p = 0.021$).

	PPA-AD	DAT	NC	ANOVA <i>p</i> -value
Participants, n	26	14	26	N/A
Age, years (SD)	67.7 (± 7.1)	71.7 (± 10.5)	67.5 (± 7.1)	0.154
Gender, % male	53.8	42.9	50.0	N/A
Education, years (SD)	16.3 (± 2.3)	16.3 (± 3.3)	15.7 (± 2.1)	0.691
Symptom duration, years (SD)	5.4 (± 2.5)	6.1 (± 2.6)	Not applicable	N / A
PPA subtype	PPA-L: 10, PPA-G: 11, Unclassifiable: 5	Not applicable	Not applicable	N / A
MMSE, %	65.1 (± 23.3)	73.6 (± 12.1)	99.6 (± 6.8)	< 0.001 ^{b,c}
WAB-AQ, % (SD)	77.1 (± 15.4)	N / A	N / A	N / A
WAB-Rep, % (SD)	59.9 (± 21.6)	N / A	99.1 (± 2.1)	N / A ^b
BNT, % (SD)	52.4 (± 25.7)	72.1 (± 27.2)	96.7 (± 3.9)	< 0.001 ^{a,b,c}
NAT-NAVS, % (SD)	87.2 (± 17.6)	N / A	98.6 (± 2.0)	N / A ^b
PPVT, % (SD)	45.3 (± 30.1)	N / A	98.6 (± 3.4)	N / A ^b

Table 1.1 Demographic and neuropsychological performance of primary progressive aphasia (PPA), dementia of the Alzheimer type (DAT), and normal control (NC) participants.

Abbreviations: PPA subtype, L = logopenic, G = agrammatic; N / A = not available; MMSE = Mini-Mental State Exam; WAB = Western Aphasia Battery; WAB-AQ = WAB aphasia quotient; WAB-Rep = WAB repetition subtest; BNT = Boston Naming Test; PPVT = Peabody Picture Vocabulary Test; NAT-NAVS = 15 non-canonical items from the Northwestern Anagram Test and 15 non-canonical items from the Northwestern Assessment of Verbs and Sentences used to measure grammatical sentence production.

Table 1.1 continued

Age, education, symptom duration, MMSE, WAB-AQ, WAB-Rep, BNT, PPVT, and NAT-NAVS are provided as means (\pm standard deviation). Gender (male), MMSE, WAB-AQ, and BNT, PPVT, and NAT-NAVS are provided as a percentage out of 100.

Two-tailed independent sample *t*-test significantly different ($p < 0.05$) between ^a PPA-AD and DAT, ^b PPA-AD and NC, or ^c between DAT and NC

PPA-AD participants had reduced connectivity compared to DAT from left IFG seed to left angular gyrus, frontal, and bilateral parietal lobule while DAT participants had reduced connectivity compared to PPA-AD to occipital cortex and fusiform gyrus (**Figure 1.1A**). From the left hippocampus seed, the PPA-AD group had reduced connectivity relative to DAT for posterior parts of the middle and inferior temporal gyrus (**Figure 1.1B**). The DAT group had more widespread reduced connectivity compared to PPA-AD group across bilateral frontal and medial cortex.

PPA-AD and DAT groups showed no between group differences for the left PCC DMN seed (**Figure 1.1C**). This leaves at least two possibilities: both groups are not different from normal or both groups have similarly altered functional connectivity. To examine this, each group was compared to 26 NC and independently showed reduced connectivity for the left PCC seed (**Figure 1.2**), supporting the notion that an altered DMN is common to both the aphasic and amnesic AD phenotypes. Differences in sample size (PPA-AD $n=26$, DAT $n=14$) may explain some of the attenuated significance compared to controls.

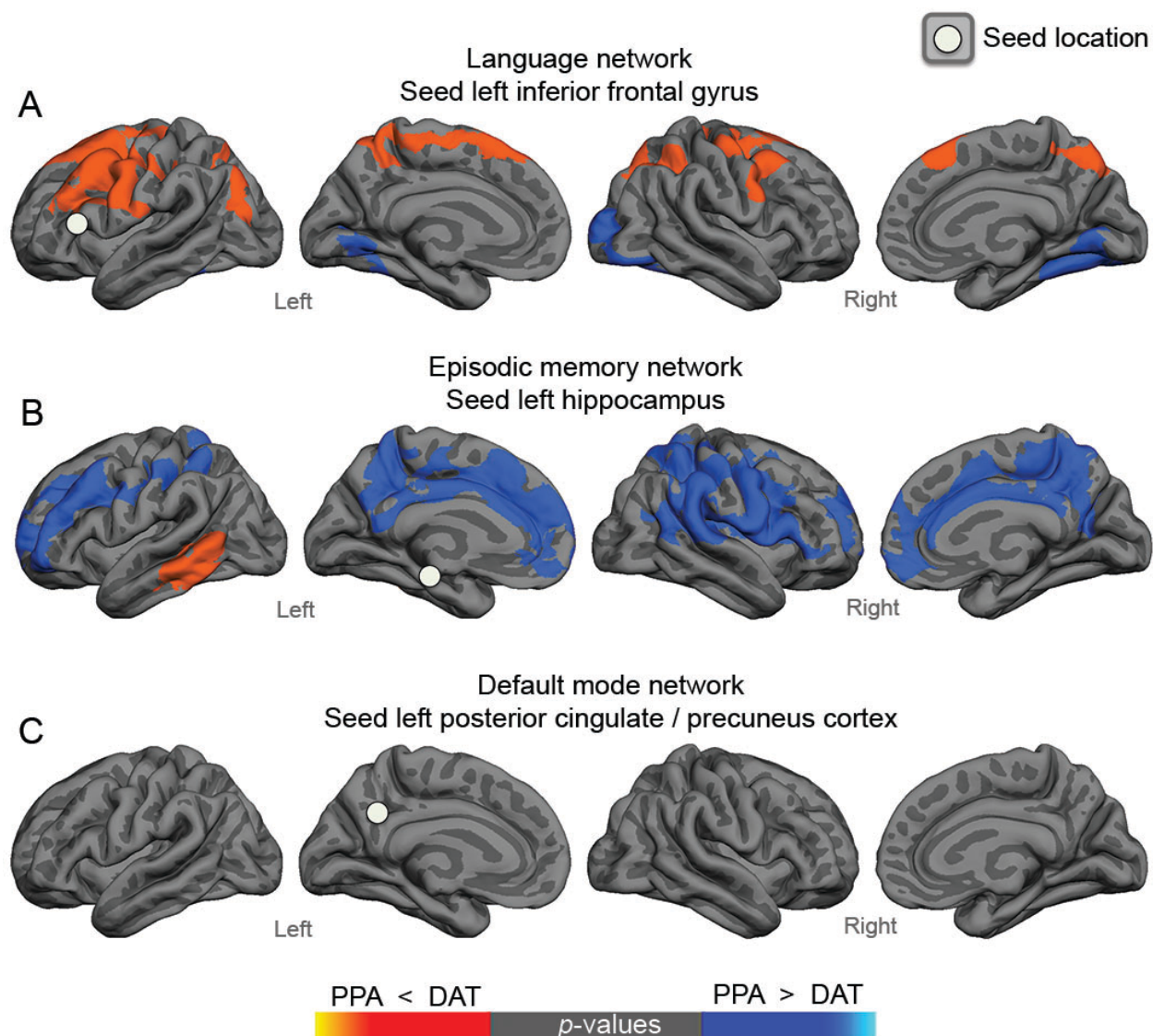


Figure 1.1 Resting-state connectivity differences between primary progressive aphasia with suspected underlying Alzheimer disease compared to dementia of the Alzheimer type. (A) Loss of functional connectivity between the IFG seed is greater in the left hemisphere for the PPA-AD group than the DAT group. **(B)** Comparing PPA-AD to DAT, the connectivity from left hippocampus to areas of left parietal and frontal cortex is more disrupted in the DAT group and a small region of left posterior lateral temporal lobe is significantly less connected in PPA-AD. **(C)** There is no difference in functional connectivity between PPA-AD and DAT groups when seeding a node of the default mode network.

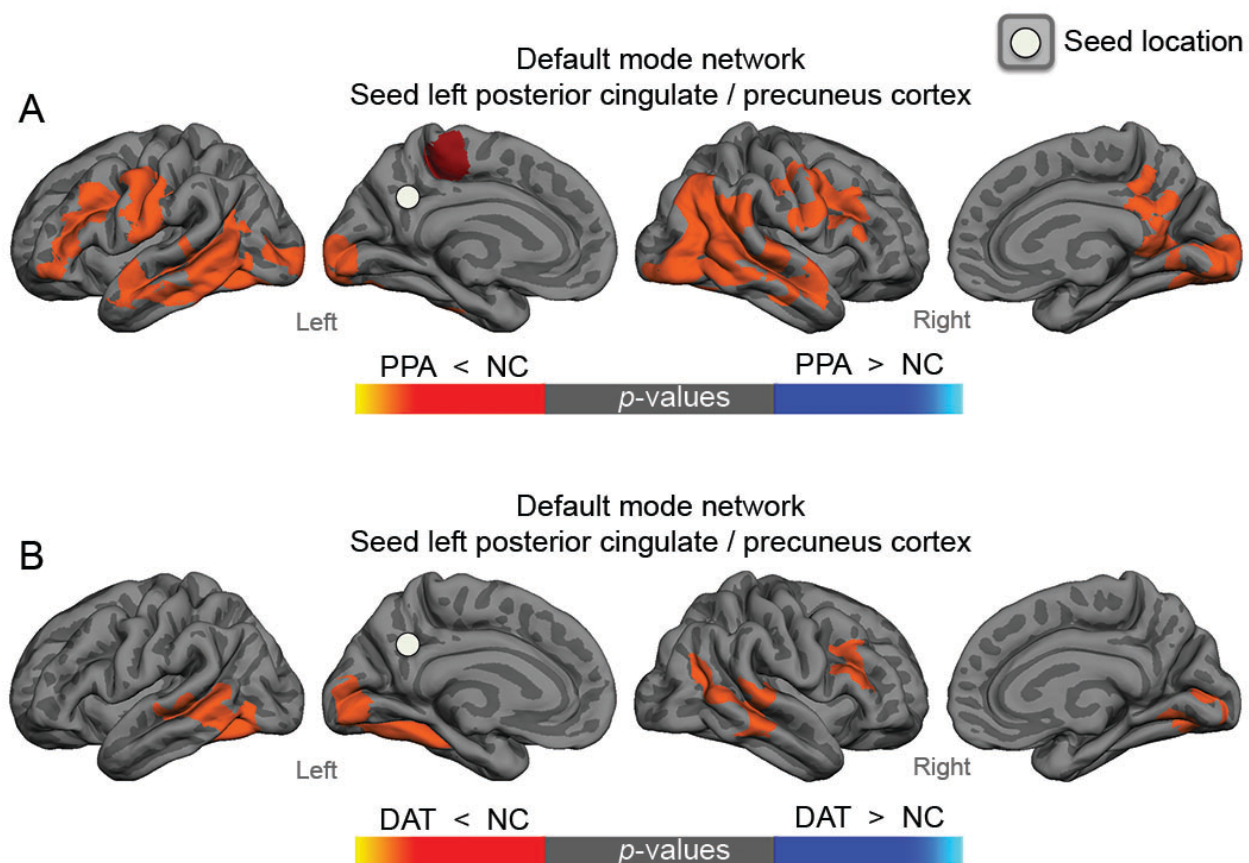


Figure 1.2. Resting-state connectivity differences from the default mode network between primary progressive aphasia with suspected underlying Alzheimer disease and dementia of the Alzheimer type groups compared to normal controls. A & B) Independently comparing PPA-AD and DAT groups to the NC group reveals a pattern of reduced connectivity in areas of frontal, parietal, and temporal cortices.

DISCUSSION

This study compared functional connectivity impairments in the aphasic versus amnesic variants of AD. The IFG node of the left hemisphere language network displayed greater reduction of connectivity in the PPA versus DAT group. In contrast, the hippocampal node of the episodic memory network showed a more widespread pattern of reduced connectivity in the DAT compared to PPA group. The amnesic and aphasic variants shared a common pattern and

magnitude of reduced connectivity within the core default mode network. The differential topography of network dysfunction provides further support for the contention that the clinical heterogeneity of dementia reflects the anatomy of functional perturbations rather than the molecular nature of the underlying neuropathology (**Mesulam, 1990; Rogalski, et al., 2016**).

Two prior studies have examined functional connectivity differences between typical amnesic versus aphasic phenotypes of AD defined by amyloid PET (**Whitwell, et al., 2014; Lehmann, et al., 2015**). Results were consistent with our lack of difference in the DMN and showed mixed findings for the language network. Lehmann and colleagues (**Lehmann, et al., 2015**) found no differences in connectivity between aphasic versus amnesic AD in the language network, executive-control network, visual network, or DMN. Whitwell and colleagues (**Whitwell, et al., 2014**) examined within network coherence and found clinically concordant differences between AD phenotypes. Neither study examined the hippocampal node of the memory network.

A limitation of the present study is the partial reliance on amyloid PET (53% of the participants) to identify AD status. An important future direction will be studies of functional networks based on autopsy proven cohorts.

Despite the fact that both aphasic and amnesic groups presumably have similar cellular neuropathology characterized by beta-amyloid and hyperphosphorylated tau (**Gefen, et al., 2012**), they showed different physiologic network vulnerabilities. This report demonstrates the potential utility of using rs-fMRI to characterize the physiological basis of clinical heterogeneity in neurodegenerative diseases.

—STUDY 2—**Tau Burden, Atrophy, and Naming in the Aphasic Variant of Alzheimer disease****Background**

Primary progressive aphasia (PPA) is an early-onset clinical dementia syndrome characterized by asymmetric atrophy of the language-dominant hemisphere. Alzheimer's disease neuropathology (AD) is present in ~40% of PPA cases. Previous cross-sectional studies examining the relationship between cognitive function, atrophy, and tau PET have reported a close relationship. However, most studies have been in amnesic AD.

Objective

To examine the relationship between flortaucipir PET burden, MRI measured cortical thickness, and naming in the aphasic variant of Alzheimer disease.

Methods

Nineteen PPA participants with suspected underlying AD underwent ¹⁸F-flortaucipir PET, structural MR imaging, and neuropsychological testing. Twelve participants received follow-up neuropsychological testing one year later. T₁-weighted Freesurfer v6.0.0 reconstructions provided Desikan-Killiany segmentations and surfaces for Rousset and Müller-Gärtner partial volume correction (PVC). Surface-wise and regional analyses examined associations between tau PET, cortical thickness, and the Boston Naming Test (BNT). We examined the association between baseline measures of tau burden and cortical thickness with the 1-year longitudinal decline in naming.

Results

Cortical atrophy and tau pathology were prominent throughout the inferior, middle, and medial temporal lobes, with a left hemisphere bias. Younger age was associated with tau PET binding in posterior temporal and parietal regions, but was not associated with cortical thickness. In a model that took into account age and thickness on tau pathology, we found widespread associations throughout all association cortices. There was a significant left-lateralized relationship between lower BNT and increased cortical thinning in the left middle and anterior temporal regions at baseline. The association between lower BNT and higher tau burden revealed a similar relationship to thinning, but included more right hemisphere regions. Twelve participants with follow-up testing revealed no significant relationship with change in BNT and baseline cortical thickness. Conversely, greater tau burden within the anterior temporal lobe predicted the decline in the BNT. Regional analyses with Rousset PVC replicated all findings.

Conclusions

MRI-derived atrophy and flortaucipir PET tau burden were strongly associated in PPA-AD, especially when considering the association of higher tau burden with younger age. Atrophy explained the decline in naming more than tau burden, while tau burden was associated with future decline.

INTRODUCTION

Primary progressive aphasia (PPA) is a clinical dementia syndrome characterized by a decline in language caused by a neurodegenerative disease. The diagnosis is made when a gradual and progressive language impairment arises in relative isolation compared to other cognitive domains (**Mesulam, 1982; 2003**). The most common neuropathology reported for PPA is frontotemporal lobar degeneration (~60%) or Alzheimer disease (AD; ~40%) (**Mesulam, et al., 2014; Rogalski, et al., 2016**). Alzheimer disease neuropathologic change (ADNC) is a pathologic diagnosis made at post-mortem examination, when the primary pathology is amyloid- β ($A\beta$) plaques and neurofibrillary tangles (NFTs) composed of hyperphosphorylated tau (**Hyman, et al., 2012; Montine, et al., 2012b**). PPA participants with ADNC or who are AD biomarker positive (PPA-AD) present with varying degrees of language dysfunction, as no language subdomain or neuropsychological test is pathognomonic and there is not a 1-to-1 correspondence between PPA subtypes and underlying pathology (**Mesulam, et al., 2014; Rogalski, et al., 2016**). PPA-AD participants are probabilistically more likely to be logopenic or agrammatic and less likely to be semantic. Probabilistically, motor speech and single word comprehension are more likely to be preserved while word-finding and naming are more likely to be impaired (**Rogalski, et al., 2016**). Over the course of disease, PPA-AD participants typically experience a decline in object naming, which could be a mixed mechanism of word-selection deficits or object recognition deficits.

Evidence from early-onset amnesic AD suggests that $A\beta$ plaques and NFTs accumulate throughout the brain years before symptom onset (**Gordon, et al., 2018**). A hypothetical model of typical late-onset sporadic AD has suggested a temporal ordering of progressively abnormal biomarkers (**Jack, et al., 2013**), including the detection of abnormal amounts of amyloid, then tau, then neurodegeneration, then clinical deficits. It is unclear to what degree these relationships between pathology and neurodegeneration or cognition exist for atypical forms of AD such as PPA and what the spatial relationship may be.

There have been several previous studies describing the topography of *in vivo* atrophy or the spatial extent of post-mortem measured pathology in PPA with AD (**Gefen, et al., 2012; Mesulam, et al., 2014; Ossenkoppele, et al., 2015a; Martersteck, et al., 2016; Ossenkoppele, et al., 2016; Bejanin, et al., 2017; Rogalski, et al., 2019**). They have found increased atrophy and NFT counts in left-lateralized language cortices and a higher ratio of language cortex-to-entorhinal NFT compared to typical amnesic AD. Further, it has been well established that clinically concordant patterns of left-lateralized atrophy can be traced to specific subdomains of language (**Rogalski, et al., 2011a; Mesulam, et al., 2019**). Since the adoption of fluorinated PET agents that bind to fibrillar amyloid-beta or hyperphosphorylated aggregates of tau, there have been few studies examining the relationship between in mild to moderate PPA with suspected underlying AD (PPA-AD) and neurodegeneration or cognition.

Rogalski and colleagues, in a longitudinal design, found atrophy continued to be greater in left language regions compared to non-language regions and PPA-AD had greater atrophy in the right hemisphere compared to amyloid negative non-semantic PPA (**Rogalski, et al., 2019**). Josephs et al. examined regional ¹⁸F-flortaucipir tau PET principal components and found subtype-specific patterns of uptake (**Josephs, et al., 2018**). La Joie and colleagues found the global intensity of tau PET could predict subsequent atrophy in a heterogeneous AD cohort (**La Joie, et al., 2020**). Additionally, they found lower baseline tau PET signal and less atrophy over time as a function of increasing patient age.

Other studies have examined tau PET associations with cognition, frequently by combining AD phenotypes into a single large group made up of visuospatial phenotypes (posterior cortical atrophy), aphasic phenotypes (PPA-AD), and typical amnesic phenotypes, all with suspected underlying AD pathology based on amyloid PET or CSF. An early study found a strong association between tau PET and FDG PET, with a correlation between a language composite and the left anterior temporal lobe (**Ossenkoppele, et al., 2016**). A follow-up study from the same

found correlations between a repetition language test composite and tau PET in left temporoparietal regions and between tau PET and measures of semantic memory in the left anterior temporal lobe (**Bejanin, et al., 2017**). Using sparse regression in a different heterogeneous AD group, a previous study found uptake in left anterior superior temporal gyrus explained 67% of variance in a composite of 5 language tests (**Phillips, et al., 2018**).

In the present study, we focused on two primary analyses: (1) to explore the relationships between atrophy and tau and their dependence on age; (2) to characterize how the decline in object naming, assessed by the Boston Naming Test (BNT), was associated with markers of atrophy and tau pathology.

We hypothesized that tau burden, assessed with flortaucipir PET, would reveal a pattern similar to atrophy. Based on post-mortem studies and recent imaging studies of early-onset AD (**La Joie, et al., 2020**), we expect higher tau burden would be associated with younger age in PPA-AD, and this discrepancy may improve the relationship between cross-sectional atrophy and tau. We hypothesized that clinicopathologic correlations between naming ability and tau PET would overlap with previously described neuroanatomic correlates of naming within the left anterior temporal lobes (**Mesulam, et al., 2013; Ossenkoppele, et al., 2016; Mesulam, et al., 2019**) and distributed language network (**Bejanin, et al., 2017; Bruffaerts, et al., 2019**). Based on current models of abnormal biomarkers (**Jack, et al., 2010; Jack, et al., 2013**), we expected atrophy to have a stronger relationship with naming than tau pathology. But we hypothesized that tau pathology would have a stronger relationship with future naming ability.

METHODS

Participants.

Nineteen individuals with a root diagnosis of PPA enrolled in Northwestern's PPA research program were identified based on having 1) ^{18}F -flortaucipir tau PET scan, 2) high resolution T₁-

and T₂-weighted structural MRI scans, 3) positive ¹⁸F-florbetapir amyloid PET or CSF indicative of AD, and 4) received neuropsychological testing. Thirty normal controls (NC) of a similar age and education underwent identical MRI pulse sequences and were used as a comparison group to identify areas of peak atrophy. Twelve of the 19 PPA participants returned a year later and received follow-up neuropsychological testing. The PPA participants were diagnosed and subtyped by a neurologist (M.M.M.) at the initial visit, based on clinical judgment and neuropsychological testing using previously described guidelines (**Mesulam, et al., 2009; Mesulam, et al., 2012**). Briefly, the PPA diagnosis was based on identification of an isolated and progressive language disorder and consistent with a neurodegenerative etiology.

Standard protocol approvals, registrations, and patient consents.

Northwestern's Institutional Review Board approved the study. Informed consent was obtained from each participant.

Neuropsychological measures

Naming was assessed with the Boston Naming Test (BNT) (**Kaplan, et al., 1983**). The BNT assesses confrontational picture naming by presenting participants with 60 line drawings of variable difficulty, administered in order from common objects (e.g. trees) to less familiar objects (e.g. a trellis) based on their frequency of occurrence in language. We chose to use the BNT to assess naming because it has proved to be reliable (**Strauss, et al., 2006**) and has routinely been used in past research and clinical settings (**Rabin, et al., 2005**). The Western Aphasia Battery (WAB) (**Kertesz, 1982**) aphasia quotient (WAB-AQ) measured aphasia severity based on naming, repetition, auditory comprehension, and spontaneous speech. The 6 most difficult items (items 10-15) from the WAB repetition subset (WAB-Rep) were used to grade repetition. Auditory lexical-semantic processing was assessed with a subset of moderately difficult items (items 157-

192) from the fourth edition of the Peabody Picture Vocabulary Test (PPVT) (**Dunn, 2007**). Grammatical processing was judged on a composite from 15 noncanonical sentences from the Northwestern Anagram Test and 15 noncanonical sentences from the Sentence Production Priming Test of the Northwestern Assessment of Verbs and Sentences (NAT-NAVS) (**Weintraub, et al., 2009**). Handedness was determined by the Edinburgh inventory (**Oldfield, 1971**).

MRI acquisition and pre-processing

MR scanning for PPA and NC participants was performed at Northwestern University (Center for Translational Imaging, Department of Radiology, Chicago, IL) on a 3.0-Tesla Siemens Prisma scanner (Siemens Healthcare, Munich, Germany). A 1mm³ T₁-weighted Magnetization Prepared Rapid Gradient Echo (MPRAGE) was acquired, using the Alzheimer's Disease Neuroimaging Initiative 3 (ADNI-3) pulse sequence, recording 176 sagittal slices with TE=2.98ms, TR=2300ms, TI=900ms, 9° flip angle, iPAT=GRAPPA 2x. A 0.8mm³ T₂-weighted Sampling Perfection with Application optimized Contrasts using different flip angle Evolution (SPACE) was acquired with online motion correction Volumetric Navigators for Prospective and Selective Reacquisition (**Tisdall, et al., 2012**), recording 208 sagittal slices with TE=564ms, TR=3200ms, iPAT=GRAPPA 2x. The T₁- and T₂-weighted volumes were denoised using an optimized nonlocal means filter (**Coupe, et al., 2008**), gradient unwarped (**Jovicich, et al., 2006**), and “de-faced” for anonymization. Importantly, the eye sockets and skull were left unchanged for the anatomical segmentation required for partial volume correction (PVC), described below.

FreeSurfer v6.0.0 was used for surface reconstruction (**Fischl, et al., 2001**; **Segonne, et al., 2007**), calculation of cortical thickness (**Fischl and Dale, 2000**), and the generation of Desikan-Killiany (**Desikan, et al., 2006**) and extracerebral segmentations (**Greve, et al., 2013**; **Greve, et al., 2016**). Briefly, FreeSurfer reconstructs estimates of the pial and white surfaces based on relative intensity differences at the boundaries of tissue classes (white-gray and pial-

CSF interfaces) (**Dale, et al., 1999**). The T_2 was conformed to 1mm^3 and rigidly registered to the T_1 with a mutual information cost function and used to further refine the outer pial-CSF surface boundary. Topological defects and inaccuracies in the estimation of surfaces were manually inspected and iteratively corrected using FreeSurfer validated guidelines (**Segonne, et al., 2007**). FreeSurfer estimated cortical thickness by calculating the average distance of the vectors perpendicular to the outer and inner surface's triangular face (**Fischl and Dale, 2000**). Each participant's native space cortical thickness estimates were vertex aligned by spherically warping to the fsaverage surface space for group statistics (**Fischl, et al., 1999**).

In addition to FreeSurfer segmentations, two additional segmentation steps were performed on the non-denoised versions of the aligned T_1 and T_2 images for the PET partial volume correction. The T_1 and co-registered T_2 image were multi-channel whole brain segmented by Statistical Parametric Mapping (SPM; Wellcome Centre for Human Neuroimaging, University College London, London, UK) version 12 for tissue class probability maps. The SUIT cerebellar atlas (**Diedrichsen, et al., 2009**) was reverse non-linear warped with DARTEL from MNI-152 space to generate segmentations of cerebellar lobules in T_1 native space.

Flortaucipir tau PET acquisition and pre-processing

Flortaucipir PET imaging was performed on a Siemens Biograph Vision PET-CT system (Siemens Healthcare, Erlangen, Germany) located at Northwestern Memorial Hospital (Department of Nuclear Medicine, Chicago, IL). PPA participants were administered a bolus intravenous injection of 10.0 mCi ($370\text{ MBq} \pm 10\%$) of flortaucipir. A low-dose computed tomography scan was acquired before PET acquisition. A dynamic PET scan recorded counts in list-mode from 80 to 100 (± 2) minutes post-injection and 4x 5-minute volumes were reconstructed, using the ADNI-3 flortaucipir protocol, with a 3D iterative ordered subset

expectation maximization (OSEM) algorithm with weighted attenuation correction and time of flight correction on a 440x440 matrix.

The four volumes were motion corrected using rigid registration and normalized cross correlation cost function with cubic spline interpolation before being averaged into a single mean volume. The process was repeated a second time, registering the four original frames to the first mean volume to avoid bias and a second mean volume was created. The second mean volume was rigidly registered with mutual information to the T_1 for correspondence with segmentations and FreeSurfer native surfaces.

Two types of partial volume correction were applied. The first was FreeSurfer's modified Müller-Gärtner PVC (**Greve, et al., 2013; Greve, et al., 2016**) for surface-wise PVC. Briefly, FreeSurfer's PVC makes several improvements on the original Rousset geometric transfer matrix (GTM) (**Rousset, et al., 1998a; Rousset, et al., 1998b**), by solving a symmetric GTM (**Sattarivand, et al., 2012**) with 0.5 mm^3 voxels containing mappings for the cortical and subcortical parcellation, extracerebral CSF, skull, and air cavity segmentations to find the values of non-cortical tissues. The non-cortical GTM solved regions were input into a Müller-Gärtner PVC that allowed each cortical ribbon voxel to independently vary and further accounted for tissue fraction effects within voxels (**Erlandsson, et al., 2012**). Corrected voxel intensities in 3D space were transformed to the native space surface by sampling along the middle 60% of every surface normal (the vector perpendicular to the white and pial surfaces, used to calculate cortical thickness). Each participant's PVC tau PET intensity values were vertex aligned by spherically warping to the fsaverage surface space.

The second method, the Rousset PVC from Baker et al. (**2017**) was used for the ROI-wise PVC. It was implemented to increase the robustness of our results and so that this work may be compared to previous or future studies that make use of it. Briefly, this PVC method operates as a standard GTM with modifications to the segmentations. It clusters extracerebral CSF, choroid

plexus, skull, and inferior cerebellar grey into areas of higher or lower uptake to avoid off-target binding to extra-cortical hotspots (ECH) that vary in anatomical location across participants (**Baker, et al., 2017**). FreeSurfer segmentations, SPM12 tissue maps, and SUIT cerebellar atlas regions are input to produce Desikan-Killiany corrected regions of interest. Based on studies of the Siemens Biograph Vision PET-CT (**van Sluis, et al., 2019**), a 3.5mm^3 point spread function was input for both PVC pipelines. The average intensity of the inferior cerebellar grey, after high ECH clusters were removed, was used as a standard uptake value ratio (SUVR) reference for both FreeSurfer surface-wise and Desikan-Killiany ROI-wise analyses.

Assessment of AD biomarkers: amyloid PET or cerebral spinal fluid

PPA participants underwent either ^{18}F -florbetapir or ^{18}F -florbetaben PET scan, or lumbar puncture with fluid collection.

For the amyloid PET acquisition, participants were given a bolus injection of 10.0 mCi (370 MBq \pm 10%) of florbetapir or 8.1 mCi (300 MBq \pm 10%) of florbetaben. Fifty minutes (florbetapir) or 90 minutes (florbetaben) post-injection, participants underwent a low-dose CT and counts were recorded for 20 minutes in dynamic listmode on a Siemens Biograph 40 TruePoint/TrueV PET-CT or Siemens Biograph Vision PET-CT (Siemens Healthcare, Erlangen, Germany). Listmode data were reconstructed into 5 minute frames with an OSEM algorithm and motion corrected with a rigid cross correlation registration to create a single mean volume.

For florebetapir and florbetaben quantification, the FreeSurfer defined volume-weighted method from (**Landau, et al., 2013**) was used. Briefly, Desikan-Killiany frontal, lateral parietal, lateral temporal, and cingulate subregion's PET intensities were weighted by their respective FreeSurfer regional volume (in mm^3). These regional SUV were added together and divided by the FreeSurfer defined whole grey cerebellar average PET intensity to derive a mean cortical SUVR. Florbetapir > 1.11 or florbetaben > 1.20 mean cortical SUVR were used for amyloid

positivity. We additionally analyzed florbetapir data with the SPM8 MRI-free PET-template approach (**Clark, et al., 2011; Fleisher, et al., 2011**) > 1.17 to confirm our findings across two different pipelines.

Cerebral spinal fluid (CSF) was obtained after a lumbar puncture and collected into polypropylene test tubes, centrifuged, and frozen within an hour of collection. Samples were shipped to Athena Diagnostics (Worcester, MA) for analysis. Measures of $A\beta_{1-42}$, t-tau, and p-tau were generated from ELISA kits (Innogenetics, Ghent, Belgium). An $A\beta_{1-42}/t$ -tau index (ATI) was calculated as $(A\beta_{1-42})/(240 + 1.18 * t\text{-tau})$. Abnormal ATI was < 1.0 and abnormal p-tau > 61 pg/ml with bands of uncertainty (borderline) from 0.8 to 1.2 ATI and from 54 to 68 pg/ml p-tau. Participants with CSF were considered eligible for the study if they fell into the “consistent with AD” category, past the borderline zones, ATI < 1.2 and p-tau > 68 pg/ml.

Statistics.

For the surface-wise analyses, a general linear model was fit at each vertex in fsaverage space. Cluster-wise corrections for multiple comparisons used a non-parametric method, Permutation Analysis of Linear Models (PALM) (**Winkler, et al., 2014**), with parameters set to cluster-forming threshold $p = 0.01$ and 0.001 , cluster-wise $p_{\text{corrected}} < 0.025$ (0.05 originally, Bonferroni corrected for each hemisphere), the Freedman-Lane method (**Freedman and Lane, 1983**), and 5000 permutations per contrast, for a familywise error (FWE) rate at 5%. The vertex-wise corrected statistical test results are displayed as FWE-corrected (FWE_c) clusters on FreeSurfer’s fsaverage surface at both cluster forming levels. We note that this permutation method is unrelated to previously reported methods popular in fMRI that were found to have artificially inflated cluster-wise extent, that relied on parametric assumptions, smoothness estimates, Monte Carlo simulations, and Gaussian random field theory (**Eklund, et al., 2016**).

Ten *a priori* regions from the Desikan-Killiany atlas that were within the left hemisphere perisylvian temporal cortex, previously found to have a strong association with progressive atrophy in PPA (**Mesulam, et al., 2014; Edland, et al., 2016**), were used in analyses between baseline BNT, GTM PVC corrected florataucipir PET, and MRI cortical thickness. The ten left hemisphere ROIs included were temporal pole, inferior frontal, fusiform, supramarginal, inferior parietal, superior temporal, middle temporal, inferior temporal, transverse temporal cortices and the banks of the superior temporal sulcus. Due to the uniform distribution of initial visit BNT scores, the non-parametric Kendall rank correlation was used as an alternative to Pearson's correlation. For the ROI-wise analyses, the Benjamini-Hochberg false discovery rate correction (FDR) (**Benjamini and Hochberg, 1995**), $q = 0.05$, was used as criterion for significance.

To assess the unique and shared variance associated with the baseline BNT in areas of the left perisylvian temporal cortex, a commonality analysis was used to decompose the R^2 statistic for the linear model $BNT_{baseline} \sim ROI_{tau} + ROI_{thickness}$. Only *a priori* ROIs that were significant after FDR correction were included. To test for a non-linear relationship for BNT on tau or thickness, a second order polynomial was added as a parameter. The fit of second order polynomial model was compared to the single parameter model with the Akaike information criterion (AIC), Bayesian information criterion (BIC), and the leave-one-out cross validation method predicted residual sum of squares (PRESS).

The calculation of the percent change in neuropsychological scores for the 12 PPA participants was annualized and calculated as the percent change with respect to the baseline visit:

$$Test_{\%change} = \frac{V2_{test} - V1_{test}}{V1_{test} \times \text{years between } V1V2} \times 100$$

$V1$ = baseline visit #1; $V2$ = return visit #2; $\text{years between } V1V2$ = exact number of days between baseline and return visits divided by 365

Differences in demographics between the PPA and NC cohorts were assessed with *t*-tests and χ^2 tests. Statistical analyses were carried out in FreeSurfer v6.0.0 (surfer.nmr.mgh.harvard.edu) and MATLAB for surface-based analyses; Python v3.6 and statsmodels package v0.9.0 for ROI-wise Kendall's rank correlation or regression; R v3.6 (The R Foundation, r-project.org) and yhat v2.0.0 for the commonality analysis (Nimon, *et al.*, 2008). Figures displaying statistics were generated using FreeSurfer, MATLAB, Python package seaborn v0.9, and R package ggseg (Mowinckel and Vidal-Pieiro, 2019).

RESULTS

Participants

Suspicion of underlying AD pathology was determined as follows: seven had a positive amyloid PET scan and eight had CSF consistent with underlying AD. Four logopenic PPA participants did not have an amyloid biomarker. All PPA and NC participants were right-handed. There were no significant demographic differences between the PPA and NC groups (all $p > 0.05$). The PPA group demographic and neuropsychological test scores are presented in **Table 2.1**. PPA participants were between 53 and 74 years old at their baseline visit. They varied from mild to moderate stages of disease, with a range on the WAB-AQ from 97 to 55 (out of 100 possible). The average follow-up neuropsychological assessment for the 12 PPA participants was 1.05 (± 0.13 SD) years after the baseline visit. The group varied on performance of the BNT, with scores from 5% to 96.7% correct at baseline, and average decline of -42.6%. Importantly, word comprehension remained intact, with 87.0% at initial visit and an average -7.0% decline over time.

	Cross-sectional group	Longitudinal group at V1	% change from V1 to V2
PPA participants, n	19	12	
Age, years (SD)	65.7 (± 6.2)	66.8 (± 5.9)	+ ~1 year
Gender, % male	73.7%	58.3%	
Education, years (SD)	16.2 (± 2.5)	15.8 (± 3.0)	
Symptom duration, years (SD)	5.8 (± 2.7)	5.5 (± 2.8)	+ ~1 year
PPA subtype	PPA-L: 11 PPA-G: 3 Mixed: 2 Unclassifiable: 3	PPA-L: 6 PPA-G: 3 Mixed: 1 Unclassifiable: 2	
WAB-AQ, % (SD)	79.7 (± 9.6)	78.5 (± 7.0)	-8.2 (± 8.3)
BNT, % (SD)	57.2 (± 30.8)	54.1 (± 21.0)	-42.6 (± 27.5)
WAB-Rep, % (SD)	59.1 (± 20.2)	56.6 (± 20.2)	-3.9 (± 23.7)
NAT-NAVS, % (SD)	58.5 (± 21.6)	53.3 (± 20.6)	-34.5 (± 49.5)
PPVT, % (SD)	87.0 (± 14.4)	83.8 (± 22.2)	-7.0 (± 18.1)

Table 2.1. Demographic and neuropsychological performance of primary progressive aphasia participants. Abbreviations: V1/V2 = Visit 1/2; SD = standard deviation; PPA = primary progressive aphasia; PPA-L = PPA logopenic subtype; PPA-G = PPA agrammatic subtype; WAB = Western Aphasia Battery; WAB-AQ = WAB aphasia quotient; BNT = Boston Naming Test; WAB-Rep = WAB repetition subset; NAT-NAVS = Northwestern Anagram Test and Northwestern Assessment of Verbs and Sentences; PPVT = Peabody Picture Vocabulary Test; ROI = region of interest; SUVR = standard uptake value ratio.

Overlapping patterns of left-lateralized atrophy and tau burden

The average tau PET binding for the PPA group was lateralized to the left hemisphere (LH), in the perisylvian temporal cortex (**Figure 2.1A**). As expected, binding was highly concentrated in the left lateral temporal and parietal lobes, with smaller clusters of signal in left

middle frontal gyrus, precuneus, and the right hemisphere posterior middle temporal gyrus. Examining the Z-score maps, the pattern of atrophy was similarly left-lateralized (**Figure 2.1B**). Cortical thinning in the PPA group was significantly different compared to the 30 NC, with significant atrophy detected across the majority of the LH (cluster $FWE_c p = 0.0002$) and right hemisphere (RH; cluster $FWE_c p = 0.0002$; **Figure 2.1C**).

Association between cortical thickness, tau burden, and age

We hypothesized that atrophy and tau would be associated, that higher tau burden would have an association with younger patient age, and that age may influence the relationship between atrophy and tau. The spatial relationship we found between thickness and age was predominantly in the bilateral inferior and middle temporal gyri, anterior temporal lobe, insula, and cuneus (LH cluster $FWE_c p = 0.0002$; RH cluster $FWE_c p = 0.0002$; **Figure 2.2A**). It did not extend further superior, to the LH supramarginal, inferior parietal, inferior frontal gyri, or precuneus where average tau PET binding can be seen overlapping with the average z-scores. We performed an analysis with age and found significant bilateral clusters at the LH and RH posterior portions of the superior temporal gyrus and the temporoparietal junction (LH cluster $FWE_c p = 0.036$; RH temporoparietal cluster $FWE_c p = 0.007$; RH frontal cluster $FWE_c p = 0.043$; **Figure 2.2B**). Subthreshold, below the multiple comparisons threshold, the relationship between age and tau burden extends to the bilateral middle frontal and inferior frontal gyri (not shown). When we added age to the previous model of tau PET on cortical thickness, in a surface-wise general linear model with $Vertex_{\tau} \sim Vertex_{thickness} + age$, we detected significant clusters across all LH and RH association cortices (LH cluster $FWE_c p = 0.0002$; RH cluster $FWE_c p = 0.0002$; **Figure 2.2C**).

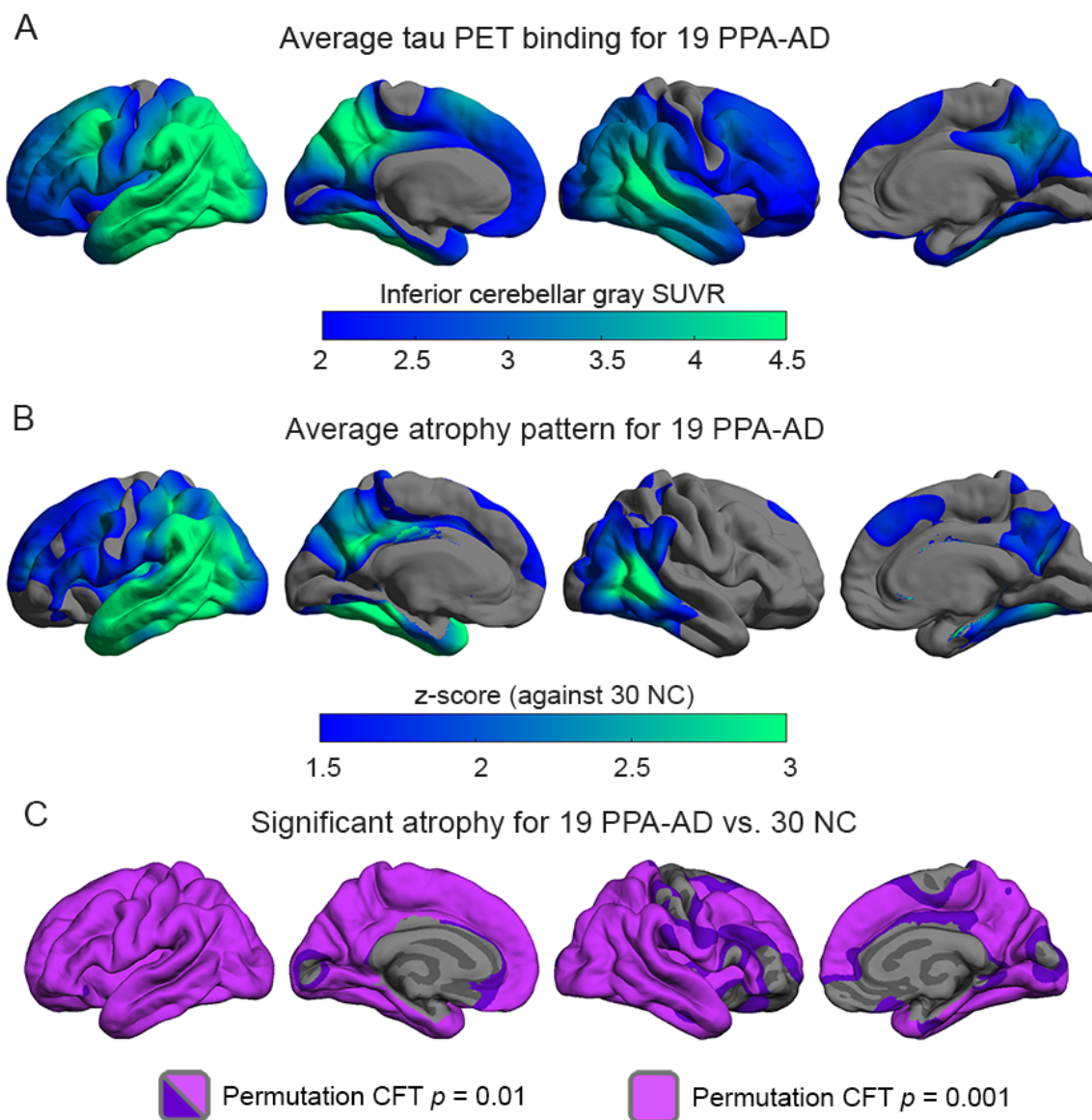


Figure 2.1. PPA-AD group patterns of tau PET and MRI atrophy. (A) The average flortaucipir PET inferior-cerebellar-gray-to-cerebral SUVR for the 19 primary progressive aphasia participants with suspected underlying AD (PPA-AD). (B) A z-score map showing regional atrophy patterns for the 19 PPA-AD. (C) The significant vertex-wise atrophy in a comparison of 19 PPA-AD vs. 30 normal controls (NC), corrected for multiple comparisons using permutation with a family wise error rate at 5% and cluster forming threshold (CFT) of $p = 0.01$ and $p = 0.001$.

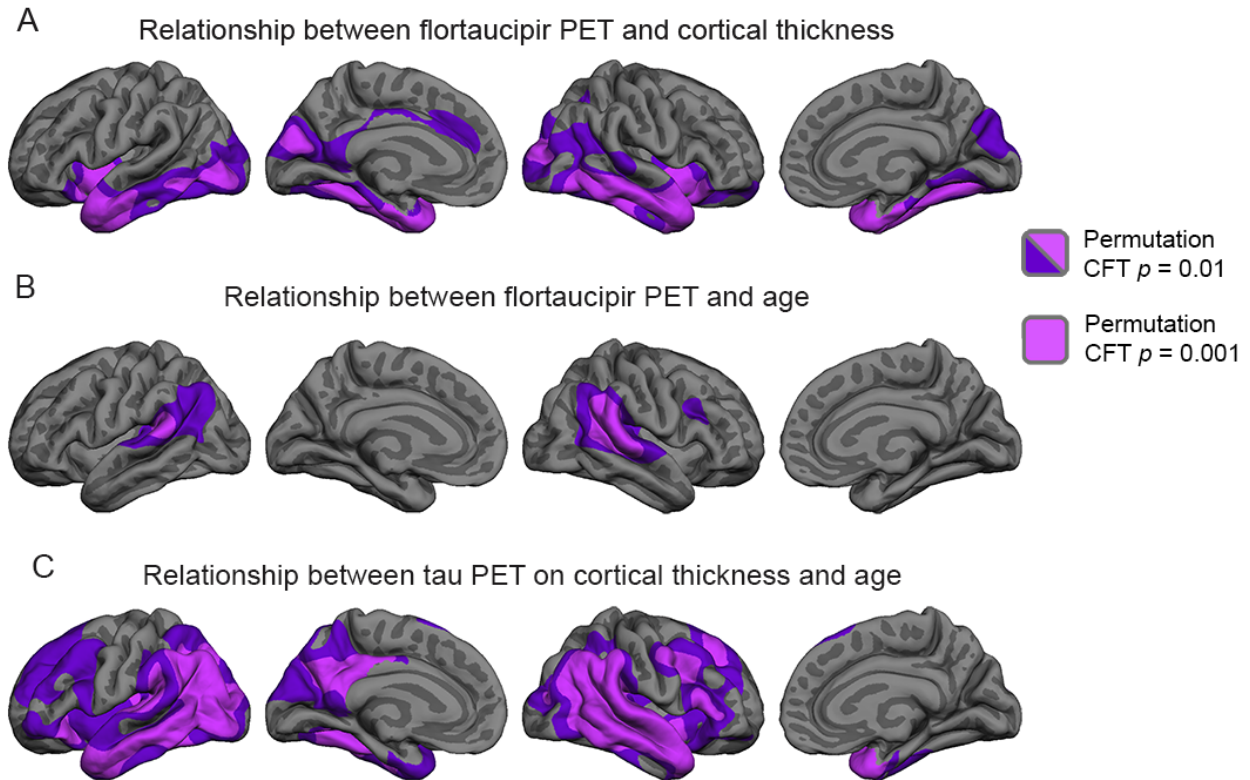


Figure 2.2. Associations of tau burden on cortical thickness and age. (A) The linear relationship between tau PET and cortical thickness is only significant in the bilateral inferior and anterior parts of the temporal lobe and does not sufficiently model the tau burden and significant cortical thinning we see in Figure 2.1. (B) The relationship between tau and age shows a markedly different spatial relationship along posterior temporal and parietal cortices. (C) The model of tau PET on cortical thickness and age is significant across the brain. Vertex-wise general linear models corrected with a permutation cluster forming threshold (CFT) of $p = 0.01$ and $p = 0.001$.

Age did not have a relationship with any other factors examined. There was no significant relationship found between age and cortical thickness (no clusters survived PALM), age and performance on the BNT_{baseline} ($\tau = -0.137$, $p = 0.419$), or age and decline on the BNT_{change} ($\tau = -0.046$, $p = 0.837$).

Atrophy and tau PET associations with baseline naming

The relationship between thinner cortex and lower BNT scores was widespread, with a left-lateralized pattern we expect for a language test (**Figure 2.3A**). Areas included the LH temporal pole, inferior and middle temporal, and orbitofrontal cortex (OFC; LH FWE_c cluster $p = 0.0062$). Only parts of the RH temporal pole, and the most anterior parts of the insula and OFC survived multiple comparisons (RH cluster FWE_c $p = 0.027$).

As we hypothesized, the spatial extent of the relationship between flortaucipir and baseline naming ability on the BNT was similar to the relationship with atrophy, with significant vertices found throughout the left and right hemisphere inferior temporal lobes, fusiform, temporal poles, OFC, and parts of each hemisphere's insula (LH cluster FWE_c $p = 0.0026$, RH cluster FWE_c $p = 0.0018$; **Figure 2.3B**). The differences between the two modalities was only found along the RH inferior temporal lobe, which was significant for the association between naming and tau.

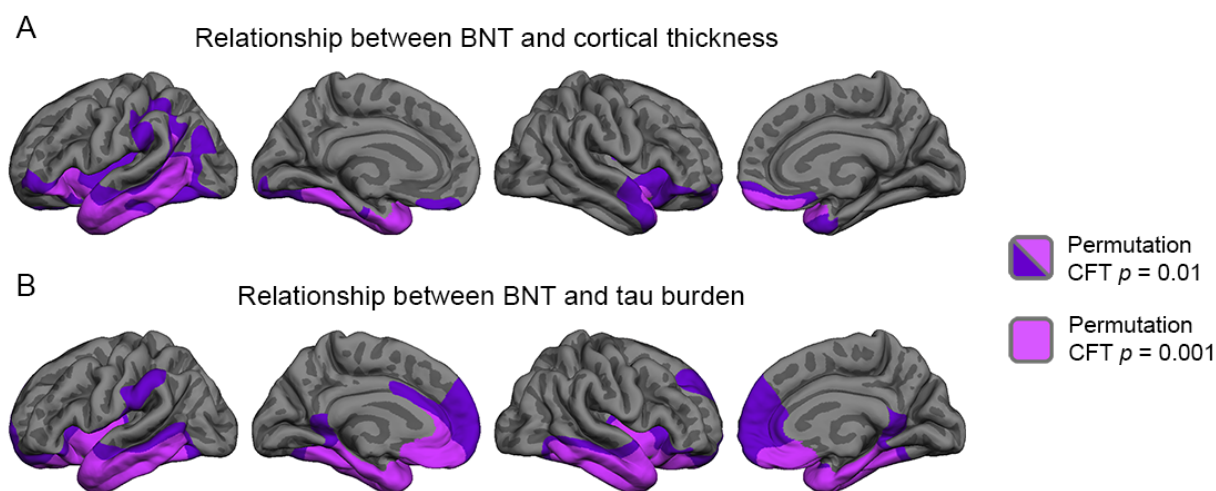
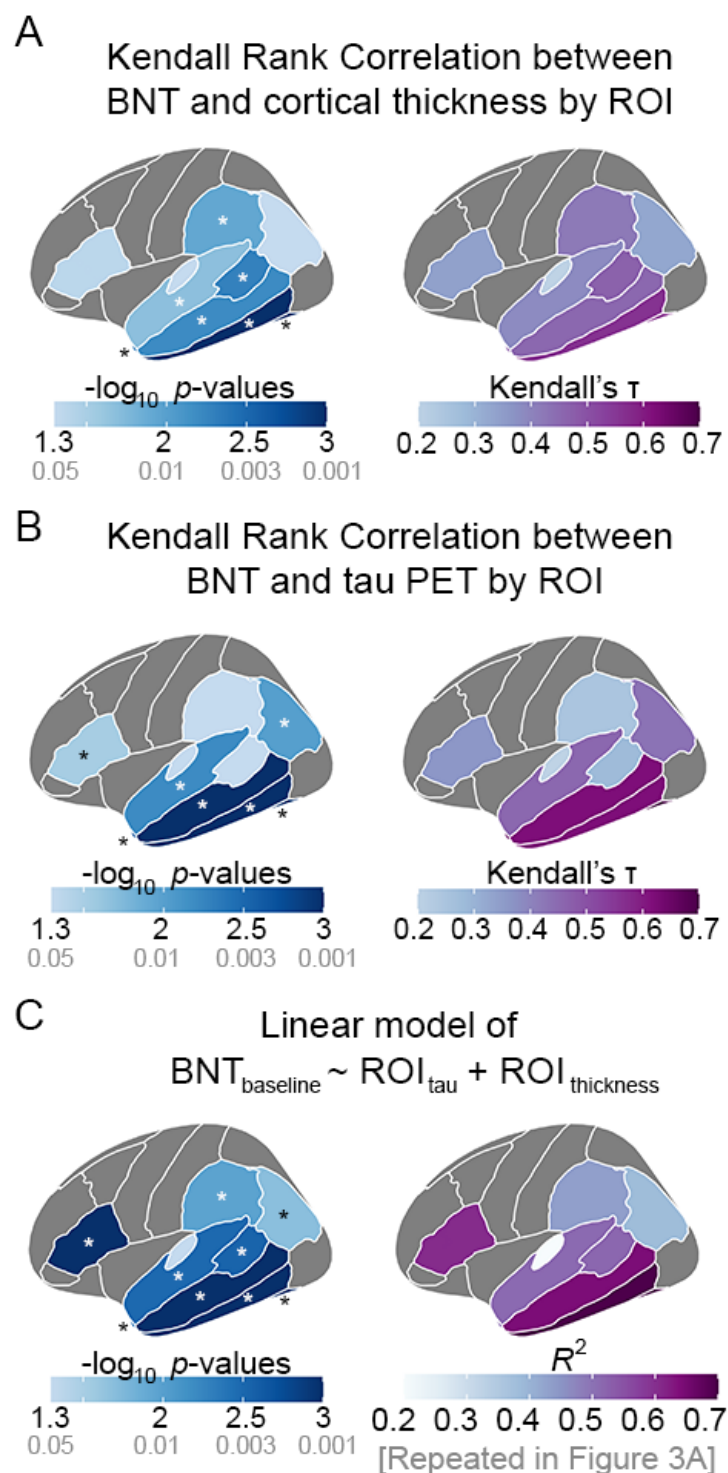


Figure 2.3. Association between baseline BNT with cortical thickness and tau burden. Displays the surface-wise significant vertices in a linear model between cross-sectional Boston Naming Test (BNT) performance and cortical thickness (**A**) or tau burden (**B**) with 19 PPA-AD participants. Corrected using permutation, with a family wise error rate 5%, with a cluster forming threshold (CFT) $p = 0.01$ and $p = 0.001$.

The ROI-wise analyses confirmed our findings above, with the GTM PVC correction technique (Baker, *et al.*, 2017) used in previous studies of tau PET. Seven out of the 10 left hemisphere language regions were significant for the correlation between $BNT_{baseline}$ and $ROI_{thickness}$ after FDR correction (Figure 2.4A). Similarly, 7 out of the 10 regions were significant for the correlation between $BNT_{baseline}$ and ROI_{tau} (Figure 2.4B). Five LH significant regions were found in common: fusiform, inferior temporal, middle temporal, superior temporal, and temporal pole. Differences were the banks of the superior temporal sulcus and supramarginal gyrus was significant for $ROI_{thickness}$ but not ROI_{tau} . Additionally, the inferior parietal and

Figure 2.4. Regional analyses confirm surface-wise findings for associations between BNT, thickness, and tau. Kendall rank correlation between baseline Boston Naming Test (BNT) performance and cortical thickness (A) or tau PET measured pathological burden (B) across 10 left hemisphere *a priori* regions of interest (ROI). The lateral brain views display the significant p -values at FDR $q=0.05$, marked with asterisks (*) and Kendall's τ . (C) The linear model predicting BNT and the accompanying R^2 values.



IFG regions were significant for ROI_{τ} and not for $ROI_{\text{thickness}}$. **Figure 2.4A+B** displays the 10 p -values and corresponding Kendall τ statistics across left hemisphere lateral brain surface for both modalities.

A linear model was fit with both ROI_{τ} and $ROI_{\text{thickness}}$ to predict BNT_{baseline} . Nine out of 10 regions survived FDR correction, with only the transverse temporal non-significant, $p = 0.593$. R^2 values are presented in **Figure 2.5A** and P -values in **Figure 2.4C**. The commonality analysis examined the shared and unique variance in the 9 significant ROIs to predict BNT_{baseline} . On average, ROI_{τ} accounted for 16% ($\pm 5\%$ SD) and $ROI_{\text{thickness}}$ accounted for 32% ($\pm 21\%$ SD) of the variance (**Figure 2.5A**). $ROI_{\tau} + ROI_{\text{thickness}}$ shared 51% ($\pm 19\%$ SD) of the variance across the LH perisylvian temporal regions. However, there were differing spatial patterns across the regions. Inferior temporal regions shared the highest degree of variance between the modalities. Cortical thickness most explained the association with BNT in the supramarginal gyrus ($R^2 = 0.43$, $\tau = 14\%$, thickness = 32%, shared = 26%) and banks of the superior temporal sulcus ($R^2 = 0.52$, $\tau = 9\%$, thickness = 71%, shared = 19%).

Temporal pole tau was the only region that exhibited a non-linear relationship with BNT decline. The association between temporal pole tau and BNT began flat and for every point on the BNT lost a greater amount more tau was found in the temporal pole (**Figure 2.5B**). The non-linear model compared to the linear model had a lower AIC, BIC, and PRESS statistic. No other region had lower scores on the model comparison statistics when a second order polynomial was added to the model.

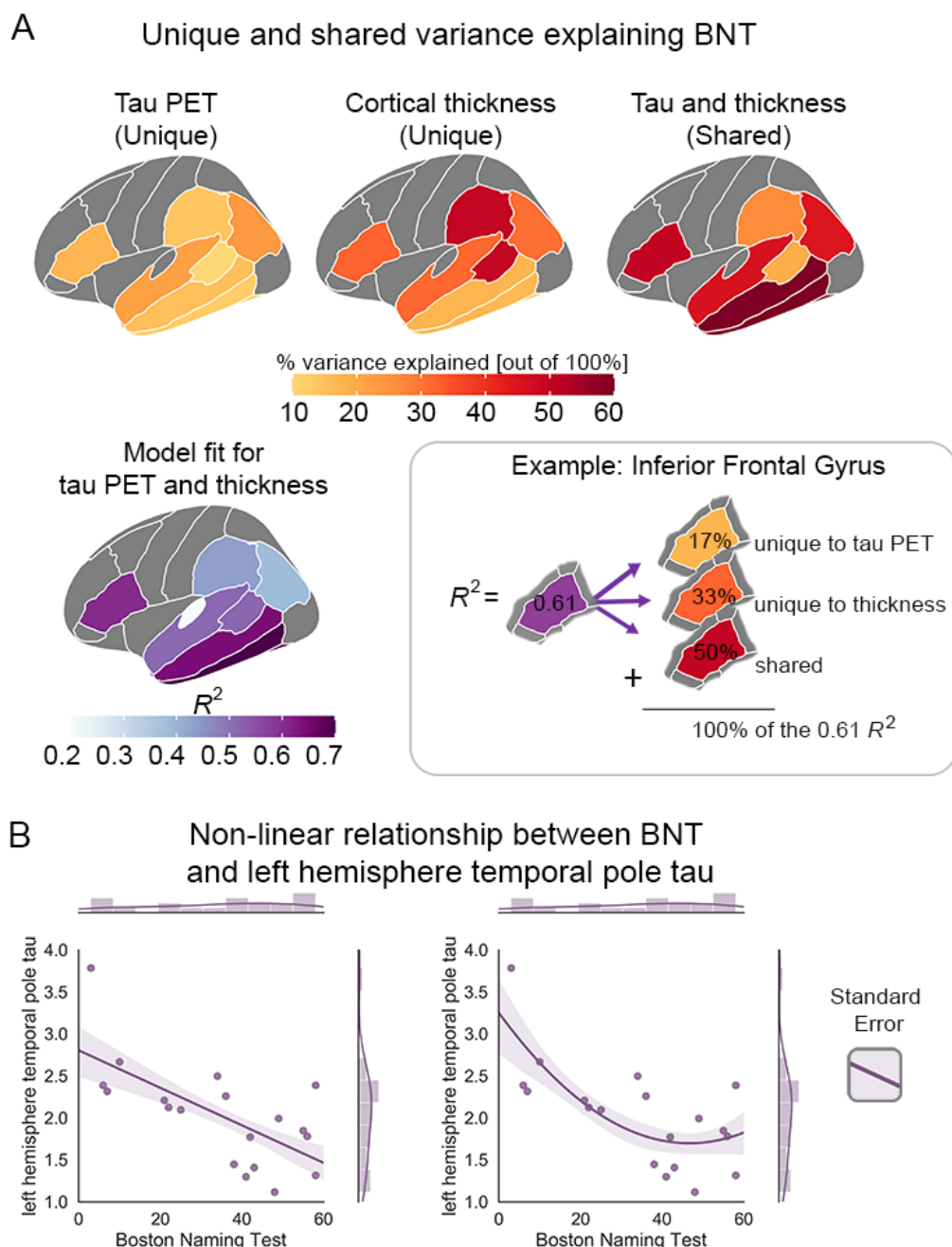


Figure 2.5. Atrophy and tau burden share and uniquely explain scores on the BNT while tau alone shows non-linear relationship. (A) The unique and shared variance in the Boston Naming Test (BNT) explained by cortical thickness and tau PET with the commonality analysis in the 9 regions that survived multiple comparisons correction. The percent variance explained is out of 100% across the same region of interest (ROI). The coefficient of determination (R^2) from the linear model of $BNT_{baseline} \sim ROI_{\tau} + ROI_{thickness}$ is displayed per ROI. (B) The BNT and left hemisphere temporal pole tau linear and non-linear regression line of best fit with shaded standard error and marginal distributions are shown. The Bayesian Information Criterion, Akaike Information Criterion, and the predicted residual error sum of squares cross-validation all favor the non-linear model.

Baseline tau PET in the left hemisphere anterior temporal lobe predicts future 1-year change in BNT

We hypothesized that future naming ability would have a stronger relationship with tau pathology than atrophy. For the group of 12 PPA-AD participants that had follow-up neuropsychological testing, the annualized percent rate of change on the BNT was not significantly related to cortical thickness in any regions (**Figure 2.6A**). Consistent with our hypothesis, significant associations were found between decline in the BNT and the left hemisphere anterior temporal lobe tau burden (LH cluster $FWE_c p = 0.017$; **Figure 2.6B**).

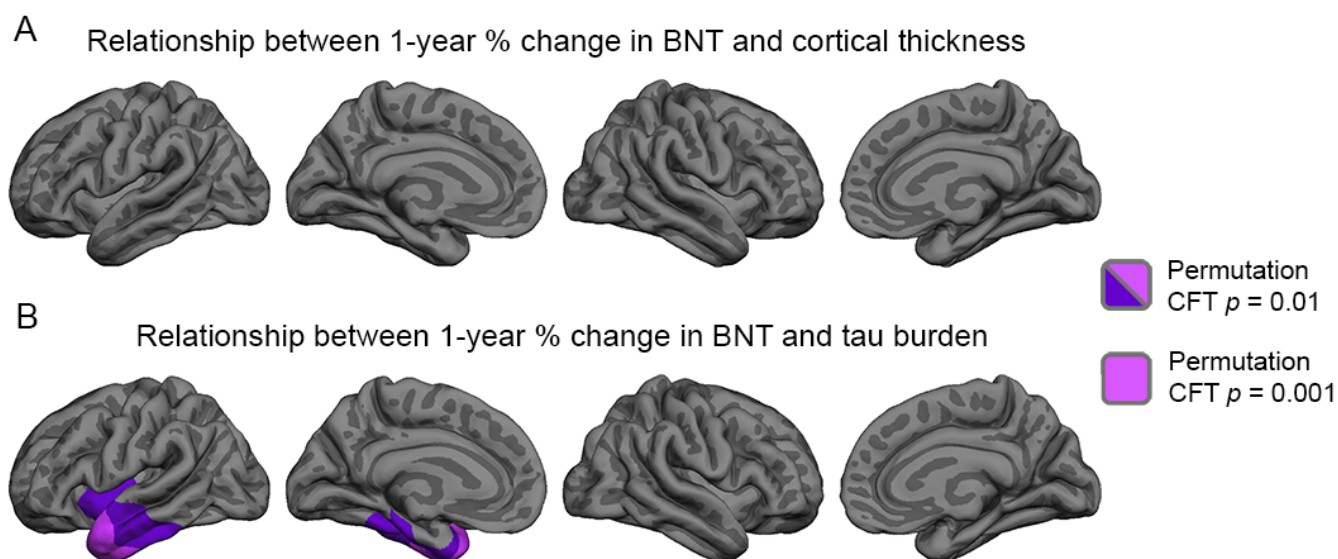


Figure 2.6. Left hemisphere anterior temporal tau is associated with future decline in naming.

(**A**) No significant relationship is found between baseline cortical thickness and the future 1-year decline on the Boston Naming Test (BNT). (**B**) The temporal pole and anterior parts of the temporal lobe tau PET measured pathological burden are significantly associated with the subsequent 1-year decline in the BNT at a permutation cluster forming threshold (CFT) of $p = 0.01$ and $p = 0.001$.

DISCUSSION

The development of PET tracers that bind to paired helical filament tau has provided the opportunity to explore the relationships with AD tau pathology, neurodegeneration, and decline in cognition. The present study examined the associations between tau burden with ¹⁸F-flortaucipir PET, structural MRI derived atrophy, age, and present or future naming performance on the Boston Naming Test in primary progressive aphasia with suspected underlying AD.

We found a left-lateralized pattern of tau deposition and atrophy in line with previous studies of tau PET and post-mortem examinations of PPA-AD (**Gefen, et al., 2012; Ossenkoppele, et al., 2016; Bejanin, et al., 2017; Josephs, et al., 2018; La Joie, et al., 2020**). The relationship between tau burden and cortical thickness was initially only significant in the inferior, middle, and medial parts of the temporal lobes. Previous cross-sectional comparisons between tau PET and MR measures of cortical thickness or FDG PET hypometabolism in elderly normal controls (**Wang, et al., 2016; Hanseeuw, et al., 2017; LaPoint, et al., 2017; Adams, et al., 2019; Harrison, et al., 2019**) or AD participants (**Bischof, et al., 2016; Ossenkoppele, et al., 2016; Xia, et al., 2017; Das, et al., 2018; Iaccarino, et al., 2018**) have found relationships, albeit modest, with either uncorrected *p*-values and rarely widespread. In the present study, we further found younger age was associated with higher tau burden in the left and right temporoparietal junction and inferior parietal lobule, spatially distinct from the relationship between atrophy and tau. In the combined linear model with tau burden on thickness and age, widespread associations were found across all cortical regions with elevated tau PET signal. Previous studies of a heterogeneous AD group have found relationships between tau PET and age in the same direction (**Ossenkoppele, et al., 2016; La Joie, et al., 2020**), but none have examined them in a model to explain tau burden on thickness. This is the first study to show this level of widespread association between tau PET, atrophy, and age in PPA-AD.

In the accepted model of large-scale distributed networks (**Mesulam, 1990; 1998**), a core synaptic hierarchy of parallel networks work together to produce cognition. Naming is likely subserved by two separate and dissociable large-scale networks: a left hemisphere dominant perisylvian temporal language network and a bilateral or right-lateralized inferotemporal/fusiform network for pictorial objects (**Damasio, 1985; Damasio, 1989; Mesulam, et al., 2013**). Naming is a complex cognitive task. Confrontational naming with an object-to-word task (i.e. the BNT) requires identification of an object, lexical retrieval to select the correct noun, phonological encoding to assemble the word sounds, and articulation to produce speech. Semantic errors can arise in the pathway even when semantic knowledge is preserved (**Hurley, et al., 2012; Mesulam, et al., 2019**). Previous studies have found the strongest associations with BNT or naming tasks in the left anterior temporal lobe measured with structural MRI (**Chan, et al., 2001; Rosen, et al., 2002; Hurley, et al., 2012; Mesulam, et al., 2013; Win, et al., 2017**), FDG PET (**Diehl, et al., 2004**), H₂¹⁵O PET (**Mummery, et al., 1999**), tau PET (**Ossenkoppele, et al., 2016; Bejanin, et al., 2017**), or post-mortem measured pathology (**Resende, et al., 2020**). Mesulam et al. (**2013**) examined PPA participants with a multidimensional naming assessment that categorized naming deficits and found anterior temporal lobe atrophy was the critical neural tissue for mediating the transcription of non-verbal concepts into verbal words. Some studies have found an association with BNT with middle and inferior temporal atrophy in PPA, amnesic AD, or frontotemporal dementia (**Chan, et al., 2001; Grossman, et al., 2004; Win, et al., 2017**), and others have used fMRI and found relationships in middle temporal and fusiform for normal controls doing a picture naming task (**Clarke and Tyler, 2014**). A recent study in PPA participants found spatially distinct anatomical correlations with the BNT when the specific types of errors were taken into account (**Bruffaerts, et al., 2019**). Semantic errors (such as mistaking intra-category related items, e.g. rhinoceros for hippopotamus) were associated with atrophy in the left fusiform,

posterior middle temporal and inferior temporal gyri, while errors of omission were confined to the anterior temporal lobes.

Based on the previous literature and due to the spatial distribution of structures involved in object-to-word naming, we hypothesized we would find a relationship between deficits in naming and increased tau or increased atrophy pre-dominantly within the left hemisphere perisylvian temporal cortex language regions. Consistent with our hypothesis, we found a significant relationship between lower BNT score and greater atrophy, found mostly throughout the inferior, middle, and anterior parts of the left temporal lobe. The relationship between BNT score and tau burden was similar, extending to more right hemisphere inferior temporal and fusiform areas thought to be responsible for object recognition. Previous studies investigating the relationship between cognition and tau PET compared to cognition and thickness in typical AD have reported more widespread associations with tau than thickness (**Digma, et al., 2019**).

The between-modality differences in association with BNT could be driven by underlying neurobiology or differences in the physical properties of the MRI and PET systems. It could be neurobiological, as hyperphosphorylated tau begins to accumulate in neurons before significant thinning and therefore shows a more widespread correlation with reduced naming. Alternatively, tau PET has inherently more spatial noise and a higher dynamic range than structural T₁-weighted thickness. Even after we attempt to reduce effects of the increased point spread function, tau PET may still have residual increased spatial smoothness and greater capturable variance compared to MRI atrophy, and therefore, have a more widespread correlation with the BNT.

With an alternate PVC algorithm and region-wise approach, we examined 10 *a priori* regions that make up the perisylvian temporal cortex that we have previously found to be optimal for tracking atrophy in PPA (**Edland, et al., 2016**) and for clinicoanatomic correlation analyses in PPA (**Mesulam, et al., 2019**). Region-wise analyses replicated the surface-wise approach and allowed us to examine the unique and shared variance explained by tau burden and atrophy on

naming performance. We found atrophy and tau in the left perisylvian temporal regions together shared the most variance in explaining naming, followed by atrophy uniquely, and tau uniquely explained the least. The present work reinforces the notion that atypical phenotypes of AD such as PPA-AD follow the tau, neurodegeneration, and subsequent loss of cognition temporal sequencing of biomarkers developed based on typical sporadic late-onset AD (**Jack, et al., 2010; Jack, et al., 2013**).

Our study had limitations. PPA-AD participants had a wide range of retrieval-based deficits and high variability of decline in naming. While tau pathology was, on average, found in the left perisylvian temporal cortex, there was still substantial variation in tau burden across individuals. This variation in naming, tau pathology, and atrophy (see (**Mesulam, et al., 2013; Mesulam, et al., 2014; Mesulam, et al., 2019**) for individual examples) made clinicoanatomic and clinicopathologic statistical comparisons ideal. But AD pathology is rarely alone, and may be found alongside TDP43, vascular, Lewy body, or argyrophilic grain pathology (**Rabinovici, et al., 2017; Nelson, et al., 2019**), which may contribute significantly and synergistically with AD pathology to explain cognition. And although early-onset forms of AD have been shown to have less co-pathology compared to late-onset AD (**Gerritsen, et al., 2016**), when co-pathology is present, it may still be important for relationships with cognition. In a study that included PPA-AD, PCA, and amnesic phenotypes of AD, a significant association was found between the BNT and density of argyrophilic thorn-shaped astrocytes at the grey/white junction in the superior temporal gyrus (**Resende, et al., 2020**). A limitation of the present study was not all pathologies could be measured and only the suspicion of underlying AD could be made based on CSF, amyloid PET and tau PET binding. Future clinicopathologic studies of cognitive decline will need to be undertaken in autopsy-proven cohorts that measure multiple pathologies.

The only disagreement between surface-wise and ROI-wise replication of the tau PET analysis was the IFG_{tau} and BNT_{baseline} correlation (**Figure 3B vs. Figure 4B**). The segmentation

of the Desikan-Killiany ROIs are based on the native-space position of the FreeSurfer generated surface, therefore it is unlikely the discrepancy is due to differences in anatomical parcellation of the IFG region. Additionally, both methods used the same reference region. The two remaining differences are the multiple comparisons correction or the partial volume correction technique.

The surface-wise analysis corrected for discoveries across LH and RH clusters and controlled the family wise error rate at 5% (probability of false positives out of all hypothesis tests conducted) while the ROI analysis was corrected for *a priori* LH regions and controlled the false discovery rate at 5% (probability of false positives out of hypothesis tests that were significant). Because the ROI analysis was restricted to *a priori* regions it may have been inadvertently more lenient (if the *a priori* regions were significant) than the whole-brain permutation FWE correction. The IFG_{tau} correlation was the weakest of the 7 out of 10 ROIs that survived FDR correction ($r = -0.364$, $p_{\text{uncorr}} = 0.03$). The $p_{\text{uncorr}} = 0.03$ would not have survived the $p < 0.01$ cluster forming threshold or $p < 0.025$ cluster-wise requirement of the permutation test. Additionally, another possible contributing factor could be small differences in the anatomical tissue class segmentations for the GTM PVC and symmetric GTM PVC for the modified Müller-Gärtner (SPM with ECHs vs. FreeSurfer, respectively).

In summary, the present study found a robust relationship between tau pathologic burden, age, and thinning. That even though PPA-AD is an early onset dementia with a different clinical presentation than typical late-onset amnesic AD, there were similar relationships to previously described studies demonstrating the close link between cross-sectional atrophy and cognition, greater than between tau and cognition. Although, for left hemisphere perisylvian regions, a considerable amount of the variance in naming (> 50%) was shared between tau and atrophy. Only tau pathology within a critical downstream node of the language network was associated with future decline in naming.

Future research should examine the importance of accumulating pathology in the networks involved in naming with more sophisticated tests of naming that are able to categorize specific errors in naming (e.g. **(Mesulam, et al., 2013)**). Future research on tau pathology and atrophy in PPA-AD will examine the longitudinal change in cortical thickness and change in tau and how measures of network integrity may influence the spread of pathology.

—GENERAL CONCLUSIONS —

We have come a long way since 1906 when Alzheimer described the first case of tangled neurofibrils and unusual plaques. The last century has been whirlwind of technological innovation. We now use massive superconducting magnets cooled by 4°K liquid helium and drive electrical currents at specific frequencies to tip spinning protons into higher energy states. And from measurements of their free induction decay, we can generate images of brain anatomy and functional physiology. We have designed specific molecular structures like keys that fit into the locks of the beta-pleated sheet structures of fibrillar amyloid or the paired helical filament structure of aggregated hyperphosphorylated tau. We bombard these molecular keys with charged particles in giant accelerators to make radionucleotides. And these high energy ligands emit beams of light invisible to the human eye, but detectable by scintillation crystals, which are excited by ionizing radiation with picosecond (one trillionth of a second) temporal resolution. It sounds like science fiction. But at the same time, a large proportion of clinical drug trials in the last two decades, especially those designed to disrupt Alzheimer pathology, have failed. There is still a great deal about the brain and the neurodegenerative pathologies so common in advancing age that we don't understand. This dissertation adds just a small brush stroke to the mosaic that is our understanding of the brain and Alzheimer disease.

The studies contained within this dissertation took a systems network-level approach to studying an aphasic form of Alzheimer disease. They were designed to contribute knowledge regarding the physiologic network integrity of PPA compared to DAT (Study 1) and to explore the relationship between tau pathology during life and the consequences of that pathology – atrophy and cognitive deficits (Study 2).

In Study 1, we examined the functional connectivity of the left-lateralized language network, the episodic memory network, and the default mode network in PPA-AD and DAT. We hypothesized that PPA-AD and DAT would have clinically concordant reductions in network communication between the associated cognitive network, language for PPA and episodic memory for DAT. Further, we hypothesized that the default mode network would be disrupted in both. There had been few previous studies of functional brain networks in PPA-AD. Previous studies had either not found differences in fMRI-derived network measures between PPA-AD vs. amnesic AD (**Lehmann, et al., 2015**) or they had examined a measure of within-network coherence and had not explored the hippocampal episodic memory network (**Whitwell, et al., 2014**). We found (1) that PPA-AD had disrupted language network functional connectivity compared to DAT, (2) DAT had reduced connectivity compared to PPA-AD of the episodic memory network, and (3) that PPA-AD and DAT had no significant differences in reduced default mode connectivity to each other, but each showed a reduced pattern of connectivity compared to normal controls.

The results we found support the notion that distinctive phenotypes of AD and related dementia phenotypes have selective physiologic network vulnerability (**Seeley, et al., 2009**). Selective vulnerability is the term used to describe the phenomena that the same underlying protein may target spatially distinct networks in different individuals. How or why pathology ‘chooses’ a network remains a mystery but potential clues are mounting. As an example, it has been found that PPA patients and first degree relatives have a higher incidence of learning disabilities, specifically dyslexia, and this may lead to a vulnerability of the left-lateralized perisylvian language network (**Rogalski, et al., 2008; Miller, et al., 2013; Rogalski, et al., 2013**). Patients with PPA may have a vulnerability of the language network that remains compensated for until it becomes the ‘locus of least resistance’ for pathology in later life. This is in line with the plasticity-based theory of AD, which postulates we pay a cost for the incredible synaptic flexibility

of neurons and metabolic milieu they encourage (**Mesulam, 2000**). And this may be especially true for the downstream transmodal association cortices (**Mesulam, 1998; Buckner, et al., 2009; Yeo, et al., 2014; Margulies, et al., 2016**), that have experienced tremendous cortical expansion in the recent hominin evolution and are untethered from sensory hierarchies (**Buckner and Krienen, 2013**). Unlike the more linear primary sensory networks, the downstream non-canonical circuitry of large-scale cognitive networks makes them highly interconnected with themselves and other cognitive networks. Like a virus in a densely interconnected urban setting, the structural core of the parallel networks described by Mesulam (**1990**) now work against us by propagating pathology non-linearly. Molecular mechanisms are proposed to be synaptic tau seeding (**Kfoury, et al., 2012; Brettschneider, et al., 2015; Goedert, et al., 2017; DeVos, et al., 2018**) and, once abnormal tau is endocytosed, the templating of normal intracellular tau into a pathologic state.

The major limitation of Study 1 is the modality, resting state fMRI connectivity, is not a true measure of the connected structural elements of the brain but rather a statistic that describes how well a network communicates between its nodes. The macrostructural connectivity of white matter that subserves information transfer in the human brain is just as important as the grey matter cell bodies. Mesulam (**2005**) said, "Nothing defines the function of a neuron more faithfully than the nature of its inputs and outputs". I remain optimistic that the subfield of neuroimaging that uses images weighted by the molecular diffusion of water (**Le Bihan, et al., 1986**) to study white matter structural connectivity will continue to improve algorithms and data collection techniques to resolve smaller and smaller fiber bundles in the brain.

The second study examined relationships between cognition, pathology, and atrophy in PPA-AD, with a similar systems level network approach. We hypothesized that naming deficits in PPA-AD would primarily be related to atrophy and tau pathology within the left-lateralized language network and connected pictorial object network. Given the importance in the left anterior temporal lobe for naming, that pathologic burden in this critical region would be especially

important for the relationship with future decline in naming. We hypothesized that cortical thickness and tau PET measured pathology would have a covarying relationship. Furthermore, that an individual's age may help explain inconsistencies in cross-sectional tau burden and thickness measurements.

We found the distribution of tau PET binding and structural T₁-weighted MRI atrophy in PPA-AD confirms the expected left-lateralized pattern based on prior autopsy and PET studies (**Gefen, et al., 2012; Mesulam, et al., 2014; Ossenkoppele, et al., 2016; Bejanin, et al., 2017; Josephs, et al., 2018**). We found relationships between both cortical thinning and tau and worsening performance on the Boston Naming Test. The relationships were throughout the left perisylvian temporal cortex for thinning, including primarily in inferior, middle, and anterior temporal regions. The pattern of tau PET with BNT was more widespread and included more of the right hemisphere. This is consistent with previous studies of tau PET on cognition in amnesic AD (**Digma, et al., 2019**), which finds correlations between cognition and tau PET are much more widespread than with cortical thickness. But the findings are at odds with the more focal finding of tau PET on measures of naming, confined to the left anterior temporal lobe, in studies with a heterogenous AD cohort (**Ossenkoppele, et al., 2016; Bejanin, et al., 2017**). Patient groups, and imaging or statistical processing choices likely played an important role in the differences. Using a statistical technique called commonality analysis to decompose the variance explained (R^2), we found that atrophy and tau PET shared the majority of the variance in the left hemisphere language network to explain naming. Furthermore, of the remaining ~50% variance, cortical thickness explained twice as much variance in the BNT than tau PET, in line with studies showing markers of neurodegeneration have a better relationship with cognition than pathology.

No other study with PPA-AD participants had examined longitudinal decline in cognition with baseline tau PET. We found the relationship between the change in naming over one year with tau PET to be confined to the left anterior temporal lobe and we could not find a relationship

between change in naming and baseline cortical thickness. Put in the context of a distributed hub and node model of naming (**Mesulam, 1990; Patterson, et al., 2007; Mesulam, et al., 2013**), the accumulation of tau pathology in the critical hub was the spatial overlapping common feature in all those participants that declined. It is likely that pathology in the distributed network also predicted future decline, but it was non-overlapping and distributed in different anatomic locations for different participants and therefore no significant relationship could be found.

The relationship between tau PET and cortical thickness has been studied in several different cohorts, from elderly cognitive normal (**Wang, et al., 2016; Hanseeuw, et al., 2017; LaPoint, et al., 2017; Adams, et al., 2019; Harrison, et al., 2019**) to early mild cognitive impairment and demented individuals with either amnesic or non-amnesic phenotypes (**Bischof, et al., 2016; Ossenkoppele, et al., 2016; Xia, et al., 2017; Das, et al., 2018; Iaccarino, et al., 2018**). Significant associations have been previously found, but they have frequently been weak, not surviving multiple comparisons correction, or in small patchy regions scattered throughout the brain. We found a relationship in the inferior, middle, and medial temporal regions between baseline thickness and tau PET. We followed this by finding a relationship with tau PET and age in a spatially distinct region, in posterior temporal and parietal cortex. In a combined model of thickness and age on tau PET, we found a widespread distributed pattern throughout most of the cortex.

This was the relationship with tau PET and atrophy we found in PPA with suspected AD. Future clinicopathologic studies of cognitive decline will need to be undertaken in autopsy-proven cohorts and with the future, yet undiscovered, molecular biomarkers that bind co-pathologies found in AD and related neurodegenerative diseases. I am encouraged by NIH funding U19 projects such as the Center Without Walls for PET Ligand Development for AD and Related Dementias. They are using *in silico* computational modelling to screen thousands of probe targets

for radioligand development, such as an alpha-synuclein PET tracer (**Lengyel-Zhand, et al., 2020**).

In summary, the present studies provide further evidence that PPA-AD may be used as a unique model system for studying AD. That there are several advantages to studying an early-onset form of AD, with less co-pathology, that has a cortical foci of pathology lateralized to one hemisphere, and cognitive deficits that are the result of accumulated pathology and subsequent neurodegeneration in multiple downstream networks. Network measures demonstrate that amnesic AD and PPA-AD have vulnerabilities in dissociable networks that match the clinical presentation. Tau pathology continues to show strong relationships with neurodegeneration, is associated with cognition, and may be more efficient for predicting future cognitive decline than atrophy.

—REFERENCES—

- Adams, J. N., Lockhart, S. N., Li, L. and Jagust, W. J. Relationships Between Tau and Glucose Metabolism Reflect Alzheimer's Disease Pathology in Cognitively Normal Older Adults. *Cerebral cortex* 2019; 29:1997-2009.
- Alzheimer, A. Über einen eigenartigen schweren Erkrankungsprozeß der Hirnrinde. *Neurologisches Centralblatt* 1906; 25:1134.
- Andrews-Hanna, J. R., Reidler, J. S., Huang, C. and Buckner, R. L. Evidence for the default network's role in spontaneous cognition. *Journal of neurophysiology* 2010a; 104:322-35.
- Andrews-Hanna, J. R., Reidler, J. S., Sepulcre, J., Poulin, R. and Buckner, R. L. Functional-anatomic fractionation of the brain's default network. *Neuron* 2010b; 65:550-62.
- Baker, S. L., Maass, A. and Jagust, W. J. Considerations and code for partial volume correcting [(18)F]-AV-1451 tau PET data. *Data Brief* 2017; 15:648-657.
- Barthel, H., Gertz, H. J., Dresel, S., Peters, O., Bartenstein, P., Buerger, K., Hiemeyer, F., Wittemer-Rump, S. M., Seibyl, J., Reiningner, C., Sabri, O. and Florbetaben Study, G. Cerebral amyloid-beta PET with florbetaben (18F) in patients with Alzheimer's disease and healthy controls: a multicentre phase 2 diagnostic study. *Lancet neurology* 2011; 10:424-35.
- Bejanin, A., Schonhaut, D. R., La Joie, R., Kramer, J. H., Baker, S. L., Sosa, N., Ayakta, N., Cantwell, A., Janabi, M., Lauriola, M., O'Neil, J. P., Gomo-Tempini, M. L., Miller, Z. A., Rosen, H. J., Miller, B. L., Jagust, W. J. and Rabinovici, G. D. Tau pathology and neurodegeneration contribute to cognitive impairment in Alzheimer's disease. *Brain : a journal of neurology* 2017; 140:3286-3300.
- Benjamini, Y. and Hochberg, Y. Controlling the false discovery rate: a practical and powerful approach to multiple testing. *Journal of the Royal Statistical Society* 1995; 57:289-300.
- Benson, D. F., Davis, R. J. and Snyder, B. D. Posterior cortical atrophy. *Archives of neurology* 1988; 45:789-93.
- Berger, H. On the electroencephalogram of man. *Electroencephalogr Clin Neurophysiol* 1931a; Suppl 28:37+.

- Berger, H. On the electroencephalogram of man. Third report. *Electroencephalogr Clin Neurophysiol* 1931b; Suppl 28:95+.
- Bischof, G. N., Jessen, F., Fliessbach, K., Dronse, J., Hammes, J., Neumaier, B., Onur, O., Fink, G. R., Kukolja, J., Drzezga, A., van Eimeren, T. and Alzheimer's Disease Neuroimaging, I. Impact of tau and amyloid burden on glucose metabolism in Alzheimer's disease. *Ann Clin Transl Neurol* 2016; 3:934-939.
- Biswal, B., Yetkin, F. Z., Haughton, V. M. and Hyde, J. S. Functional connectivity in the motor cortex of resting human brain using echo-planar MRI. *Magnetic resonance in medicine : official journal of the Society of Magnetic Resonance in Medicine / Society of Magnetic Resonance in Medicine* 1995; 34:537-41.
- Blessed, G., Tomlinson, B. E. and Roth, M. The association between quantitative measures of dementia and of senile change in the cerebral grey matter of elderly subjects. *Br J Psychiatry* 1968; 114:797-811.
- Braak, H., Braak, E. and Bohl, J. Staging of Alzheimer-Related Cortical Destruction. *Eur Neurol* 1993; 33:403-408.
- Braak, H. and Del Tredici, K. The pathological process underlying Alzheimer's disease in individuals under thirty. *Acta neuropathologica* 2011; 121:171-81.
- Braak, H., Thal, D. R., Ghebremedhin, E. and Del Tredici, K. Stages of the pathologic process in Alzheimer disease: age categories from 1 to 100 years. *Journal of neuropathology and experimental neurology* 2011; 70:960-9.
- Brettschneider, J., Del Tredici, K., Lee, V. M. and Trojanowski, J. Q. Spreading of pathology in neurodegenerative diseases: a focus on human studies. *Nature reviews. Neuroscience* 2015; 16:109-20.
- Bruffaerts, R., Schaefferbeke, J., De Weer, A. S., Nelissen, N., Dries, E., Van Bouwel, K., Sieben, A., Bergmans, B., Swinnen, C., Pijnenburg, Y., Sunaert, S., Vandenbulcke, M. and Vandenberghe, R. Multivariate analysis reveals anatomical correlates of naming errors in primary progressive aphasia. *Neurobiology of aging* 2019;
- Buckner, R. L., Andrews-Hanna, J. R. and Schacter, D. L. The brain's default network: anatomy, function, and relevance to disease. *Annals of the New York Academy of Sciences* 2008; 1124:1-38.

- Buckner, R. L. and Krienen, F. M. The evolution of distributed association networks in the human brain. *Trends in cognitive sciences* 2013; 17:648-65.
- Buckner, R. L., Sepulcre, J., Talukdar, T., Krienen, F. M., Liu, H., Hedden, T., Andrews-Hanna, J. R., Sperling, R. A. and Johnson, K. A. Cortical hubs revealed by intrinsic functional connectivity: mapping, assessment of stability, and relation to Alzheimer's disease. *The Journal of neuroscience : the official journal of the Society for Neuroscience* 2009; 29:1860-73.
- Chan, D., Fox, N. C., Scahill, R. I., Crum, W. R., Whitwell, J. L., Leschziner, G., Rossor, A. M., Stevens, J. M., Cipolotti, L. and Rossor, M. N. Patterns of temporal lobe atrophy in semantic dementia and Alzheimer's disease. *Annals of neurology* 2001; 49:433-42.
- Chien, D. T., Bahri, S., Szardenings, A. K., Walsh, J. C., Mu, F., Su, M. Y., Shankle, W. R., Elizarov, A. and Kolb, H. C. Early clinical PET imaging results with the novel PHF-tau radioligand [F-18]-T807. *Journal of Alzheimer's disease : JAD* 2013; 34:457-68.
- Choi, S. R., Golding, G., Zhuang, Z., Zhang, W., Lim, N., Hefti, F., Benedum, T. E., Kilbourn, M. R., Skovronsky, D. and Kung, H. F. Preclinical properties of 18F-AV-45: a PET agent for Abeta plaques in the brain. *Journal of nuclear medicine : official publication, Society of Nuclear Medicine* 2009; 50:1887-94.
- Clark, C. M., Pontecorvo, M. J., Beach, T. G., Bedell, B. J., Coleman, R. E., Doraiswamy, P. M., Fleisher, A. S., Reiman, E. M., Sabbagh, M. N., Sadowsky, C. H., Schneider, J. A., Arora, A., Carpenter, A. P., Flitter, M. L., Joshi, A. D., Krautkramer, M. J., Lu, M., Mintun, M. A., Skovronsky, D. M. and Group, A.-A. S. Cerebral PET with florbetapir compared with neuropathology at autopsy for detection of neuritic amyloid-beta plaques: a prospective cohort study. *Lancet neurology* 2012; 11:669-78.
- Clark, C. M., Schneider, J. A., Bedell, B. J., Beach, T. G., Bilker, W. B., Mintun, M. A., Pontecorvo, M. J., Hefti, F., Carpenter, A. P., Flitter, M. L., Krautkramer, M. J., Kung, H. F., Coleman, R. E., Doraiswamy, P. M., Fleisher, A. S., Sabbagh, M. N., Sadowsky, C. H., Reiman, E. P., Zehntner, S. P., Skovronsky, D. M. and Group, A. A. S. Use of florbetapir-PET for imaging beta-amyloid pathology. *JAMA : the journal of the American Medical Association* 2011; 305:275-83.
- Clarke, A. and Tyler, L. K. Object-specific semantic coding in human perirhinal cortex. *The Journal of neuroscience : the official journal of the Society for Neuroscience* 2014; 34:4766-75.

- Coupe, P., Yger, P., Prima, S., Hellier, P., Kervrann, C. and Barillot, C. An optimized blockwise nonlocal means denoising filter for 3-D magnetic resonance images. *IEEE transactions on medical imaging* 2008; 27:425-41.
- Crutch, S. J., Schott, J. M., Rabinovici, G. D., Murray, M., Snowden, J. S., van der Flier, W. M., Dickerson, B. C., Vandenberghe, R., Ahmed, S., Bak, T. H., Boeve, B. F., Butler, C., Cappa, S. F., Ceccaldi, M., de Souza, L. C., Dubois, B., Felician, O., Galasko, D., Graff-Radford, J., Graff-Radford, N. R., Hof, P. R., Krolak-Salmon, P., Lehmann, M., Magnin, E., Mendez, M. F., Nestor, P. J., Onyike, C. U., Pelak, V. S., Pijnenburg, Y., Primativo, S., Rossor, M. N., Ryan, N. S., Scheltens, P., Shakespeare, T. J., Suarez Gonzalez, A., Tang-Wai, D. F., Yong, K. X. X., Carrillo, M., Fox, N. C., Alzheimer's Association, I. A. A. s. D. and Associated Syndromes Professional Interest, A. Consensus classification of posterior cortical atrophy. *Alzheimer's & dementia : the journal of the Alzheimer's Association* 2017; 13:870-884.
- Dale, A. M., Fischl, B. and Sereno, M. I. Cortical surface-based analysis. I. Segmentation and surface reconstruction. *NeuroImage* 1999; 9:179-94.
- Damasio, A. The brain binds entities and events by multiregional activation from convergence zones. *Neural Computation* 1989; 1:123-132.
- Damasio, A. R. Disorders of complex visual processing: agnosias, achromatopsia, Balint's syndrome, and related difficulties of orientation and construction. M.-M. Mesulam, editor. Philadelphia 1985.
- Das, S. R., Xie, L., Wisse, L. E. M., Ittyerah, R., Tustison, N. J., Dickerson, B. C., Yushkevich, P. A., Wolk, D. A. and Alzheimer's Disease Neuroimaging, I. Longitudinal and cross-sectional structural magnetic resonance imaging correlates of AV-1451 uptake. *Neurobiology of aging* 2018; 66:49-58.
- De Luca, M., Beckmann, C. F., De Stefano, N., Matthews, P. M. and Smith, S. M. fMRI resting state networks define distinct modes of long-distance interactions in the human brain. *NeuroImage* 2006; 29:1359-67.
- Desikan, R. S., Segonne, F., Fischl, B., Quinn, B. T., Dickerson, B. C., Blacker, D., Buckner, R. L., Dale, A. M., Maguire, R. P., Hyman, B. T., Albert, M. S. and Killiany, R. J. An automated labeling system for subdividing the human cerebral cortex on MRI scans into gyral based regions of interest. *NeuroImage* 2006; 31:968-80.
- DeVos, S. L., Corjuc, B. T., Oakley, D. H., Nobuhara, C. K., Bannon, R. N., Chase, A., Commins, C., Gonzalez, J. A., Dooley, P. M., Frosch, M. P. and Hyman, B. T. Synaptic

- Tau Seeding Precedes Tau Pathology in Human Alzheimer's Disease Brain. *Frontiers in neuroscience* 2018; 12:267.
- Diedrichsen, J., Balsters, J. H., Flavell, J., Cussans, E. and Ramnani, N. A probabilistic MR atlas of the human cerebellum. *NeuroImage* 2009; 46:39-46.
- Diehl, J., Grimmer, T., Drzezga, A., Riemenschneider, M., Forstl, H. and Kurz, A. Cerebral metabolic patterns at early stages of frontotemporal dementia and semantic dementia. A PET study. *Neurobiology of aging* 2004; 25:1051-6.
- Digma, L. A., Madsen, J. R., Reas, E. T., Dale, A. M., Brewer, J. B., Banks, S. J. and Alzheimer's Disease Neuroimaging, I. Tau and atrophy: domain-specific relationships with cognition. *Alzheimers Res Ther* 2019; 11:65.
- Dunn, L. M. D., Douglas M. Peabody Picture Vocabulary Test. Toronto, Ontario, Canada: Pearson Assessments; 2007.
- Edelman, G. M. Group selection and phasic re-entrant signalling: a theory of higher brain function. . G. M. Edelman and V. B. Mountcastle, editors. Cambridge, Massachusetts: MIT Press; 1978.
- Edelman, G. M. *Neural Darwinism: The Theory of Neuronal Group Selection* New York: Basic Books; 1987.
- Edland, S. D., Ard, M. C., Sridhar, J., Cobia, D., Martersteck, A., Mesulam, M. M. and Rogalski, E. J. Proof of concept demonstration of optimal composite MRI endpoints for clinical trials. *Alzheimer's & dementia* 2016; 2:177-181.
- Eichling, J. O., Raichle, M. E., Grubb, R. L., Jr., Larson, K. B. and Ter-Pogossian, M. M. In vivo determination of cerebral blood volume with radioactive oxygen-15 in the monkey. *Circ Res* 1975; 37:707-14.
- Eklund, A., Nichols, T. E. and Knutsson, H. Cluster failure: Why fMRI inferences for spatial extent have inflated false-positive rates. *Proceedings of the National Academy of Sciences of the United States of America* 2016; 113:7900-5.
- Erlandsson, K., Buvat, I., Pretorius, P. H., Thomas, B. A. and Hutton, B. F. A review of partial volume correction techniques for emission tomography and their applications in neurology, cardiology and oncology. *Physics in medicine and biology* 2012; 57:R119-59.

- Felleman, D. J. and Van Essen, D. C. Distributed hierarchical processing in the primate cerebral cortex. *Cerebral cortex* 1991; 1:1-47.
- Fischl, B. and Dale, A. M. Measuring the thickness of the human cerebral cortex from magnetic resonance images. *Proceedings of the National Academy of Sciences of the United States of America* 2000; 97:11050-5.
- Fischl, B., Liu, A. and Dale, A. M. Automated manifold surgery: constructing geometrically accurate and topologically correct models of the human cerebral cortex. *IEEE transactions on medical imaging* 2001; 20:70-80.
- Fischl, B., Sereno, M. I., Tootell, R. B. and Dale, A. M. High-resolution intersubject averaging and a coordinate system for the cortical surface. *Human brain mapping* 1999; 8:272-84.
- Fleisher, A. S., Chen, K., Liu, X., Roontiva, A., Thiyyagura, P., Ayutyanont, N., Joshi, A. D., Clark, C. M., Mintun, M. A., Pontecorvo, M. J., Doraiswamy, P. M., Johnson, K. A., Skovronsky, D. M. and Reiman, E. M. Using positron emission tomography and florbetapir F18 to image cortical amyloid in patients with mild cognitive impairment or dementia due to Alzheimer disease. *Archives of neurology* 2011; 68:1404-11.
- Fox, N. C. and Freeborough, P. A. Brain atrophy progression measured from registered serial MRI: validation and application to Alzheimer's disease. *Journal of magnetic resonance imaging : JMRI* 1997; 7:1069-75.
- Fox, P. T. The coupling controversy. *NeuroImage* 2012; 62:594-601.
- Freeborough, P. A. and Fox, N. C. The boundary shift integral: an accurate and robust measure of cerebral volume changes from registered repeat MRI. *IEEE transactions on medical imaging* 1997; 16:623-9.
- Freedman, D. and Lane, D. A nonstochastic interpretation of reported significance levels. *Journal of Business & Economic Statistics* 1983; 1:292-298.
- Frisoni, G. B., Ritchie, C., Carrera, E., Nilsson, P., Ousset, P. J., Molinuevo, J. L., Dubois, B., Scheltens, P. and Minoshima, S. Re-aligning scientific and lay narratives of Alzheimer's disease. *Lancet neurology* 2019; 18:918-919.
- Gefen, T., Gasho, K., Rademaker, A., Lalehzari, M., Weintraub, S., Rogalski, E., Wieneke, C., Bigio, E., Geula, C. and Mesulam, M. M. Clinically concordant variations of Alzheimer pathology in aphasic versus amnesic dementia. *Brain : a journal of neurology* 2012; 135:1554-65.

- Gerritsen, A. A., Bakker, C., Verhey, F. R., de Vugt, M. E., Melis, R. J., Koopmans, R. T. and team, C. s. Prevalence of Comorbidity in Patients With Young-Onset Alzheimer Disease Compared With Late-Onset: A Comparative Cohort Study. *J Am Med Dir Assoc* 2016; 17:318-23.
- Gilbert, D. T. and Wilson, T. D. Propection: experiencing the future. *Science* 2007; 317:1351-4.
- Glasser, M. F., Coalson, T. S., Robinson, E. C., Hacker, C. D., Harwell, J., Yacoub, E., Ugurbil, K., Andersson, J., Beckmann, C. F., Jenkinson, M., Smith, S. M. and Van Essen, D. C. A multi-modal parcellation of human cerebral cortex. *Nature* 2016; 536:171-178.
- Goedert, M., Eisenberg, D. S. and Crowther, R. A. Propagation of Tau Aggregates and Neurodegeneration. *Annu Rev Neurosci* 2017; 40:189-210.
- Gordon, B. A., Blazey, T. M., Su, Y., Hari-Raj, A., Dincer, A., Flores, S., Christensen, J., McDade, E., Wang, G., Xiong, C., Cairns, N. J., Hassenstab, J., Marcus, D. S., Fagan, A. M., Jack, C. R., Jr., Hornbeck, R. C., Paumier, K. L., Ances, B. M., Berman, S. B., Brickman, A. M., Cash, D. M., Chhatwal, J. P., Correia, S., Forster, S., Fox, N. C., Graff-Radford, N. R., la Fougere, C., Levin, J., Masters, C. L., Rossor, M. N., Salloway, S., Saykin, A. J., Schofield, P. R., Thompson, P. M., Weiner, M. M., Holtzman, D. M., Raichle, M. E., Morris, J. C., Bateman, R. J. and Benzinger, T. L. S. Spatial patterns of neuroimaging biomarker change in individuals from families with autosomal dominant Alzheimer's disease: a longitudinal study. *Lancet neurology* 2018; 17:241-250.
- Gorno-Tempini, M. L., Hillis, A. E., Weintraub, S., Kertesz, A., Mendez, M., Cappa, S. F., Ogar, J. M., Rohrer, J. D., Black, S., Boeve, B. F., Manes, F., Dronkers, N. F., Vandenberghe, R., Rascovsky, K., Patterson, K., Miller, B. L., Knopman, D. S., Hodges, J. R., Mesulam, M. M. and Grossman, M. Classification of primary progressive aphasia and its variants. *Neurology* 2011; 76:1006-14.
- Greicius, M. D., Srivastava, G., Reiss, A. L. and Menon, V. Default-mode network activity distinguishes Alzheimer's disease from healthy aging: evidence from functional MRI. *Proceedings of the National Academy of Sciences of the United States of America* 2004; 101:4637-42.
- Greve, D. N. and Fischl, B. Accurate and robust brain image alignment using boundary-based registration. *NeuroImage* 2009; 48:63-72.
- Greve, D. N., Salat, D. H., Bowen, S. L., Izquierdo-Garcia, D., Schultz, A. P., Catana, C., Becker, J. A., Svarer, C., Knudsen, G. M., Sperling, R. A. and Johnson, K. A. Different partial volume correction methods lead to different conclusions: An F-FDG-PET study of aging. *NeuroImage* 2016; 132:334-343.

- Greve, D. N., Svarer, C., Fisher, P. M., Feng, L., Hansen, A. E., Baare, W., Rosen, B., Fischl, B. and Knudsen, G. M. Cortical surface-based analysis reduces bias and variance in kinetic modeling of brain PET data. *NeuroImage* 2013;
- Grossman, M., McMillan, C., Moore, P., Ding, L., Glosser, G., Work, M. and Gee, J. What's in a name: voxel-based morphometric analyses of MRI and naming difficulty in Alzheimer's disease, frontotemporal dementia and corticobasal degeneration. *Brain : a journal of neurology* 2004; 127:628-49.
- Hanseeuw, B. J., Betensky, R. A., Schultz, A. P., Papp, K. V., Mormino, E. C., Sepulcre, J., Bark, J. S., Cosio, D. M., LaPoint, M., Chhatwal, J. P., Rentz, D. M., Sperling, R. A. and Johnson, K. A. Fluorodeoxyglucose metabolism associated with tau-amyloid interaction predicts memory decline. *Annals of neurology* 2017; 81:583-596.
- Harrison, T. M., La Joie, R., Maass, A., Baker, S. L., Swinnerton, K., Fenton, L., Mellinger, T. J., Edwards, L., Pham, J., Miller, B. L., Rabinovici, G. D. and Jagust, W. J. Longitudinal tau accumulation and atrophy in aging and Alzheimer disease. *Annals of neurology* 2019; 85:229-240.
- Hof, P. R., Archin, N., Osmand, A. P., Dougherty, J. H., Wells, C., Bouras, C. and Morrison, J. H. Posterior cortical atrophy in Alzheimer's disease: analysis of a new case and re-evaluation of a historical report. *Acta neuropathologica* 1993; 86:215-23.
- Hof, P. R., Bouras, C., Constantinidis, J. and Morrison, J. H. Balint's syndrome in Alzheimer's disease: specific disruption of the occipito-parietal visual pathway. *Brain Res* 1989; 493:368-75.
- Hurley, R. S., Paller, K. A., Rogalski, E. J. and Mesulam, M. M. Neural mechanisms of object naming and word comprehension in primary progressive aphasia. *The Journal of neuroscience : the official journal of the Society for Neuroscience* 2012; 32:4848-55.
- Hyman, B. T., Phelps, C. H., Beach, T. G., Bigio, E. H., Cairns, N. J., Carrillo, M. C., Dickson, D. W., Duyckaerts, C., Frosch, M. P., Masliah, E., Mirra, S. S., Nelson, P. T., Schneider, J. A., Thal, D. R., Thies, B., Trojanowski, J. Q., Vinters, H. V. and Montine, T. J. National Institute on Aging-Alzheimer's Association guidelines for the neuropathologic assessment of Alzheimer's disease. *Alzheimers & Dementia* 2012; 8:1-13.
- Iaccarino, L., Tammewar, G., Ayakta, N., Baker, S. L., Bejanin, A., Boxer, A. L., Gorno-Tempini, M. L., Janabi, M., Kramer, J. H., Lazaris, A., Lockhart, S. N., Miller, B. L., Miller, Z. A., O'Neil, J. P., Ossenkoppele, R., Rosen, H. J., Schonhaut, D. R., Jagust, W. J. and Rabinovici, G. D. Local and distant relationships between amyloid, tau and neurodegeneration in Alzheimer's Disease. *NeuroImage. Clinical* 2018; 17:452-464.

- Ikonomic, M. D., Klunk, W. E., Abrahamson, E. E., Mathis, C. A., Price, J. C., Tsopelas, N. D., Lopresti, B. J., Ziolk, S., Bi, W., Paljug, W. R., Debnath, M. L., Hope, C. E., Isanski, B. A., Hamilton, R. L. and DeKosky, S. T. Post-mortem correlates of in vivo PiB-PET amyloid imaging in a typical case of Alzheimer's disease. *Brain : a journal of neurology* 2008; 131:1630-45.
- Irwin, D. J., McMillan, C. T., Toledo, J. B., Arnold, S. E., Shaw, L. M., Wang, L. S., Van Deerlin, V., Lee, V. M., Trojanowski, J. Q. and Grossman, M. Comparison of cerebrospinal fluid levels of tau and Abeta 1-42 in Alzheimer disease and frontotemporal degeneration using 2 analytical platforms. *Arch Neurol* 2012; 69:1018-25.
- Jack, C. R., Jr. Brain Atrophy on Magnetic Resonance Imaging as a Biomarker of Neurodegeneration. *JAMA neurology* 2016; 73:1179-1182.
- Jack, C. R., Jr. Preclinical Alzheimer's disease: a valid concept. *Lancet neurology* 2020; 19:31.
- Jack, C. R., Jr., Bennett, D. A., Blennow, K., Carrillo, M. C., Dunn, B., Haeblerlein, S. B., Holtzman, D. M., Jagust, W., Jessen, F., Karlawish, J., Liu, E., Molinuevo, J. L., Montine, T., Phelps, C., Rankin, K. P., Rowe, C. C., Scheltens, P., Siemers, E., Snyder, H. M., Sperling, R. and Contributors. NIA-AA Research Framework: Toward a biological definition of Alzheimer's disease. *Alzheimer's & dementia : the journal of the Alzheimer's Association* 2018; 14:535-562.
- Jack, C. R., Jr., Bennett, D. A., Blennow, K., Carrillo, M. C., Feldman, H. H., Frisoni, G. B., Hampel, H., Jagust, W. J., Johnson, K. A., Knopman, D. S., Petersen, R. C., Scheltens, P., Sperling, R. A. and Dubois, B. A/T/N: An unbiased descriptive classification scheme for Alzheimer disease biomarkers. *Neurology* 2016a; 87:539-47.
- Jack, C. R., Jr., Knopman, D. S., Jagust, W. J., Petersen, R. C., Weiner, M. W., Aisen, P. S., Shaw, L. M., Vemuri, P., Wiste, H. J., Weigand, S. D., Lesnick, T. G., Pankratz, V. S., Donohue, M. C. and Trojanowski, J. Q. Tracking pathophysiological processes in Alzheimer's disease: an updated hypothetical model of dynamic biomarkers. *Lancet neurology* 2013; 12:207-16.
- Jack, C. R., Jr., Knopman, D. S., Jagust, W. J., Shaw, L. M., Aisen, P. S., Weiner, M. W., Petersen, R. C. and Trojanowski, J. Q. Hypothetical model of dynamic biomarkers of the Alzheimer's pathological cascade. *Lancet neurology* 2010; 9:119-28.
- Jack, C. R., Jr., Twomey, C. K., Zinsmeister, A. R., Sharbrough, F. W., Petersen, R. C. and Cascino, G. D. Anterior temporal lobes and hippocampal formations: normative volumetric measurements from MR images in young adults. *Radiology* 1989; 172:549-54.

- Jack, C. R., Jr., Wiste, H. J., Weigand, S. D., Knopman, D. S., Mielke, M. M., Vemuri, P., Lowe, V., Senjem, M. L., Gunter, J. L., Reyes, D., Machulda, M. M., Roberts, R. and Petersen, R. C. Different definitions of neurodegeneration produce similar amyloid/neurodegeneration biomarker group findings. *Brain : a journal of neurology* 2015; 138:3747-59.
- Jack, C. R., Jr., Wiste, H. J., Weigand, S. D., Themeau, T. M., Lowe, V. J., Knopman, D. S., Gunter, J. L., Senjem, M. L., Jones, D. T., Kantarci, K., Machulda, M. M., Mielke, M. M., Roberts, R. O., Vemuri, P., Reyes, D. A. and Petersen, R. C. Defining imaging biomarker cut points for brain aging and Alzheimer's disease. *Alzheimer's & dementia : the journal of the Alzheimer's Association* 2016b;
- Jagust, W., Jack, C. R., Jr., Bennett, D. A., Blennow, K., Haeblerlein, S. B., Holtzman, D. M., Jessen, F., Karlawish, J., Liu, E., Molinuevo, J. L., Montine, T., Phelps, C., Rankin, K. P., Rowe, C. C., Scheltens, P., Siemers, E. and Sperling, R. "Alzheimer's disease" is neither "Alzheimer's clinical syndrome" nor "dementia". *Alzheimer's & dementia : the journal of the Alzheimer's Association* 2019; 15:153-157.
- Ji, J. L., Spronk, M., Kulkarni, K., Repovs, G., Anticevic, A. and Cole, M. W. Mapping the human brain's cortical-subcortical functional network organization. *NeuroImage* 2019; 185:35-57.
- Johnson, J. K., Head, E., Kim, R., Starr, A. and Cotman, C. W. Clinical and pathological evidence for a frontal variant of Alzheimer disease. *Archives of neurology* 1999; 56:1233-9.
- Josephs, K. A., Martin, P. R., Botha, H., Schwarz, C. G., Duffy, J. R., Clark, H. M., Machulda, M. M., Graff-Radford, J., Weigand, S. D., Senjem, M. L., Utianski, R. L., Drubach, D. A., Boeve, B. F., Jones, D. T., Knopman, D. S., Petersen, R. C., Jack, C. R., Jr., Lowe, V. J. and Whitwell, J. L. [(18) F]AV-1451 tau-PET and primary progressive aphasia. *Annals of neurology* 2018; 83:599-611.
- Joshi, A. D., Pontecorvo, M. J., Clark, C. M., Carpenter, A. P., Jennings, D. L., Sadowsky, C. H., Adler, L. P., Kovnat, K. D., Seibyl, J. P., Arora, A., Saha, K., Burns, J. D., Lowrey, M. J., Mintun, M. A., Skovronsky, D. M. and Florbetapir, F. S. I. Performance characteristics of amyloid PET with florbetapir F 18 in patients with alzheimer's disease and cognitively normal subjects. *Journal of nuclear medicine : official publication, Society of Nuclear Medicine* 2012; 53:378-84.
- Jovicich, J., Czanner, S., Greve, D., Haley, E., van der Kouwe, A., Gollub, R., Kennedy, D., Schmitt, F., Brown, G., Macfall, J., Fischl, B. and Dale, A. Reliability in multi-site structural MRI studies: effects of gradient non-linearity correction on phantom and human data. *NeuroImage* 2006; 30:436-43.

- Jureus, A., Swahn, B. M., Sandell, J., Jeppsson, F., Johnson, A. E., Johnstrom, P., Neelissen, J. A., Sunnemark, D., Farde, L. and Svensson, S. P. Characterization of AZD4694, a novel fluorinated Abeta plaque neuroimaging PET radioligand. *Journal of neurochemistry* 2010; 114:784-94.
- Kaplan, E., Goodglass, H. and Weintraub, S. Boston naming test. Philadelphia: Lea & Febiger; 1983.
- Kertesz, A. Western Aphasia Battery: The Psychological Corporation; 1982.
- Kesslak, J. P., Nalcioglu, O. and Cotman, C. W. Quantification of magnetic resonance scans for hippocampal and parahippocampal atrophy in Alzheimer's disease. *Neurology* 1991; 41:51-4.
- Kfoury, N., Holmes, B. B., Jiang, H., Holtzman, D. M. and Diamond, M. I. Trans-cellular propagation of Tau aggregation by fibrillar species. *The Journal of biological chemistry* 2012; 287:19440-51.
- Klunk, W. E., Engler, H., Nordberg, A., Wang, Y., Blomqvist, G., Holt, D. P., Bergstrom, M., Savitcheva, I., Huang, G. F., Estrada, S., Ausen, B., Debnath, M. L., Barletta, J., Price, J. C., Sandell, J., Lopresti, B. J., Wall, A., Koivisto, P., Antoni, G., Mathis, C. A. and Langstrom, B. Imaging brain amyloid in Alzheimer's disease with Pittsburgh Compound-B. *Annals of neurology* 2004; 55:306-19.
- Kraepelin, E. *Psychiatrie: Ein Lehrbuch für Studierende und Ärzte, Klinische Psychiatrie*, part 1. Leipzig, Germany 1910.
- La Joie, R., Visani, A. V., Baker, S. L., Brown, J. A., Bourakova, V., Cha, J., Chaudhary, K., Edwards, L., Iaccarino, L., Janabi, M., Lesman-Segev, O. H., Miller, Z. A., Perry, D. C., O'Neil, J. P., Pham, J., Rojas, J. C., Rosen, H. J., Seeley, W. W., Tsai, R. M., Miller, B. L., Jagust, W. J. and Rabinovici, G. D. Prospective longitudinal atrophy in Alzheimer's disease correlates with the intensity and topography of baseline tau-PET. *Sci Transl Med* 2020; 12:
- Landau, S. M., Breault, C., Joshi, A. D., Pontecorvo, M., Mathis, C. A., Jagust, W. J., Mintun, M. A. and Alzheimer's Disease Neuroimaging, I. Amyloid-beta imaging with Pittsburgh compound B and florbetapir: comparing radiotracers and quantification methods. *Journal of nuclear medicine : official publication, Society of Nuclear Medicine* 2013; 54:70-7.
- LaPoint, M. R., Chhatwal, J. P., Sepulcre, J., Johnson, K. A., Sperling, R. A. and Schultz, A. P. The association between tau PET and retrospective cortical thinning in clinically normal elderly. *NeuroImage* 2017; 157:612-622.

- Lauterbur, P. C. Image Formation by Induced Local Interactions: Examples Employing Nuclear Magnetic Resonance. *Nature* 1973; 242:190-191.
- Le Bihan, D., Breton, E., Lallemand, D., Grenier, P., Cabanis, E. and Laval-Jeantet, M. MR imaging of intravoxel incoherent motions: application to diffusion and perfusion in neurologic disorders. *Radiology* 1986; 161:401-7.
- Lehky, S. R. and Sejnowski, T. J. Network model of shape-from-shading: neural function arises from both receptive and projective fields. *Nature* 1988; 333:452-4.
- Lehmann, M., Madison, C., Ghosh, P. M., Miller, Z. A., Greicius, M. D., Kramer, J. H., Coppola, G., Miller, B. L., Jagust, W. J., Gorno-Tempini, M. L., Seeley, W. W. and Rabinovici, G. D. Loss of functional connectivity is greater outside the default mode network in nonfamilial early-onset Alzheimer's disease variants. *Neurobiology of aging* 2015; 36:2678-86.
- Lengyel-Zhand, Z., Ferrie, J. J., Janssen, B., Hsieh, C. J., Graham, T., Xu, K. Y., Haney, C. M., Lee, V. M., Trojanowski, J. Q., Petersson, E. J. and Mach, R. H. Synthesis and characterization of high affinity fluorogenic alpha-synuclein probes. *Chem Commun (Camb)* 2020;
- Lustig, C., Snyder, A. Z., Bhakta, M., O'Brien, K. C., McAvoy, M., Raichle, M. E., Morris, J. C. and Buckner, R. L. Functional deactivations: change with age and dementia of the Alzheimer type. *Proceedings of the National Academy of Sciences of the United States of America* 2003; 100:14504-9.
- Maass, A., Landau, S., Baker, S. L., Horng, A., Lockhart, S. N., La Joie, R., Rabinovici, G. D., Jagust, W. J. and Alzheimer's Disease Neuroimaging, I. Comparison of multiple tau-PET measures as biomarkers in aging and Alzheimer's disease. *NeuroImage* 2017; 157:448-463.
- Margulies, D. S., Ghosh, S. S., Goulas, A., Falkiewicz, M., Huntenburg, J. M., Langs, G., Bezgin, G., Eickhoff, S. B., Castellanos, F. X., Petrides, M., Jefferies, E. and Smallwood, J. Situating the default-mode network along a principal gradient of macroscale cortical organization. *Proceedings of the National Academy of Sciences of the United States of America* 2016; 113:12574-12579.
- Martersteck, A., Murphy, C., Rademaker, A., Wieneke, C., Weintraub, S., Chen, K., Mesulam, M. M., Rogalski, E. and Alzheimer's Disease Neuroimaging, I. Is in vivo amyloid distribution asymmetric in primary progressive aphasia? *Annals of neurology* 2016; 79:496-501.

- McKhann, G., Drachman, D., Folstein, M., Katzman, R., Price, D. and Stadlan, E. M. Clinical diagnosis of Alzheimer's disease: report of the NINCDS-ADRDA Work Group under the auspices of Department of Health and Human Services Task Force on Alzheimer's Disease. *Neurology* 1984; 34:939-44.
- McKhann, G. M., Knopman, D. S., Chertkow, H., Hyman, B. T., Jack, C. R., Jr., Kawas, C. H., Klunk, W. E., Koroshetz, W. J., Manly, J. J., Mayeux, R., Mohs, R. C., Morris, J. C., Rossor, M. N., Scheltens, P., Carrillo, M. C., Thies, B., Weintraub, S. and Phelps, C. H. The diagnosis of dementia due to Alzheimer's disease: recommendations from the National Institute on Aging-Alzheimer's Association workgroups on diagnostic guidelines for Alzheimer's disease. *Alzheimer's & dementia : the journal of the Alzheimer's Association* 2011; 7:263-9.
- Mesulam, M. Representation, inference, and transcendent encoding in neurocognitive networks of the human brain. *Annals of neurology* 2008; 64:367-78.
- Mesulam, M. Defining neurocognitive networks in the BOLD new world of computed connectivity. *Neuron* 2009; 62:1-3.
- Mesulam, M., Wieneke, C., Rogalski, E., Cobia, D., Thompson, C. and Weintraub, S. Quantitative template for subtyping primary progressive aphasia. *Archives of neurology* 2009; 66:1545-51.
- Mesulam, M. M. Slowly progressive aphasia without generalized dementia. *Annals of neurology* 1982; 11:592-8.
- Mesulam, M. M. Large-scale neurocognitive networks and distributed processing for attention, language, and memory. *Annals of neurology* 1990; 28:597-613.
- Mesulam, M. M. From sensation to cognition. *Brain : a journal of neurology* 1998; 121 (Pt 6):1013-52.
- Mesulam, M. M. A plasticity-based theory of the pathogenesis of Alzheimer's disease. *Annals of the New York Academy of Sciences* 2000; 924:42-52.
- Mesulam, M. M. Primary progressive aphasia--a language-based dementia. *The New England journal of medicine* 2003; 349:1535-42.
- Mesulam, M. M., Rader, B. M., Sridhar, J., Nelson, M. J., Hyun, J., Rademaker, A., Geula, C., Bigio, E. H., Thompson, C. K., Gefen, T. D., Weintraub, S. and Rogalski, E. J. Word

- comprehension in temporal cortex and Wernicke area: A PPA perspective. *Neurology* 2019; 92:e224-e233.
- Mesulam, M. M., Thompson, C. K., Weintraub, S. and Rogalski, E. J. The Wernicke conundrum and the anatomy of language comprehension in primary progressive aphasia. *Brain : a journal of neurology* 2015; 138:2423-37.
- Mesulam, M. M., Weintraub, S., Rogalski, E. J., Wieneke, C., Geula, C. and Bigio, E. H. Asymmetry and heterogeneity of Alzheimer's and frontotemporal pathology in primary progressive aphasia. *Brain : a journal of neurology* 2014; 137:1176-92.
- Mesulam, M. M., Wieneke, C., Hurley, R., Rademaker, A., Thompson, C. K., Weintraub, S. and Rogalski, E. J. Words and objects at the tip of the left temporal lobe in primary progressive aphasia. *Brain : a journal of neurology* 2013; 136:601-18.
- Mesulam, M. M., Wieneke, C., Thompson, C., Rogalski, E. and Weintraub, S. Quantitative classification of primary progressive aphasia at early and mild impairment stages. *Brain : a journal of neurology* 2012; 135:1537-53.
- Miller, Z. A., Mandelli, M. L., Rankin, K. P., Henry, M. L., Babiak, M. C., Frazier, D. T., Lobach, I. V., Bettcher, B. M., Wu, T. Q., Rabinovici, G. D., Graff-Radford, N. R., Miller, B. L. and Gorno-Tempini, M. L. Handedness and language learning disability differentially distribute in progressive aphasia variants. *Brain : a journal of neurology* 2013; 136:3461-73.
- Montine, T. J., Phelps, C. H., Beach, T. G., Bigio, E. H., Cairns, N. J., Dickson, D. W., Duyckaerts, C., Frosch, M. P., Masliah, E., Mirra, S. S., Nelson, P. T., Schneider, J. A., Thal, D. R., Trojanowski, J. Q., Vinters, H. V. and Hyman, B. T. National Institute on Aging-Alzheimer's Association guidelines for the neuropathologic assessment of Alzheimer's disease: a practical approach. *Acta neuropathologica* 2012a; 123:1-11.
- Montine, T. J., Phelps, C. H., Beach, T. G., Bigio, E. H., Cairns, N. J., Dickson, D. W., Duyckaerts, C., Frosch, M. P., Masliah, E., Mirra, S. S., Nelson, P. T., Schneider, J. A., Thal, D. R., Trojanowski, J. Q., Vinters, H. V., Hyman, B. T., National Institute on, A. and Alzheimer's, A. National Institute on Aging-Alzheimer's Association guidelines for the neuropathologic assessment of Alzheimer's disease: a practical approach. *Acta neuropathologica* 2012b; 123:1-11.
- Mowinckel, A. and Vidal-Pieiro, D. Visualisation of Brain Statistics with R-packages ggseg and ggseg3d. *arXiv* 2019;

- Mummery, C. J., Patterson, K., Wise, R. J., Vandenberghe, R., Price, C. J. and Hodges, J. R. Disrupted temporal lobe connections in semantic dementia. *Brain : a journal of neurology* 1999; 122 (Pt 1):61-73.
- Murray, M. E., Graff-Radford, N. R., Ross, O. A., Petersen, R. C., Duara, R. and Dickson, D. W. Neuropathologically defined subtypes of Alzheimer's disease with distinct clinical characteristics: a retrospective study. *Lancet neurology* 2011; 10:785-96.
- Nelissen, N., Van Laere, K., Thurfjell, L., Owenius, R., Vandenbulcke, M., Koole, M., Bormans, G., Brooks, D. J. and Vandenberghe, R. Phase 1 study of the Pittsburgh compound B derivative 18F-flutemetamol in healthy volunteers and patients with probable Alzheimer disease. *Journal of nuclear medicine : official publication, Society of Nuclear Medicine* 2009; 50:1251-9.
- Nelson, P. T., Dickson, D. W., Trojanowski, J. Q., Jack, C. R., Boyle, P. A., Arfanakis, K., Rademakers, R., Alafuzoff, I., Attems, J., Brayne, C., Coyle-Gilchrist, I. T. S., Chui, H. C., Fardo, D. W., Flanagan, M. E., Halliday, G., Hokkanen, S. R. K., Hunter, S., Jicha, G. A., Katsumata, Y., Kawas, C. H., Keene, C. D., Kovacs, G. G., Kukull, W. A., Levey, A. I., Makkinejad, N., Montine, T. J., Murayama, S., Murray, M. E., Nag, S., Rissman, R. A., Seeley, W. W., Sperling, R. A., White lli, C. L., Yu, L. and Schneider, J. A. Limbic-predominant age-related TDP-43 encephalopathy (LATE): consensus working group report. *Brain : a journal of neurology* 2019; 142:1503-1527.
- Nimon, K., Lewis, M., Kane, R. and Haynes, R. M. An R package to compute commonality coefficients in the multiple regression case: an introduction to the package and a practical example. *Behav Res Methods* 2008; 40:457-66.
- Ohm, D. T., Fought, A. J., Rademaker, A., Kim, G., Sridhar, J., Coventry, C., Gefen, T., Weintraub, S., Bigio, E., Mesulam, M. M., Rogalski, E. and Geula, C. Neuropathologic basis of in vivo cortical atrophy in the aphasic variant of Alzheimer's disease. *Brain Pathol* 2020; 30:332-344.
- Oldfield, R. C. The assessment and analysis of handedness: the Edinburgh inventory. *Neuropsychologia* 1971; 9:97-113.
- Opris, I., Chang, S. and Noga, B. R. What Is the Evidence for Inter-laminar Integration in a Prefrontal Cortical Minicolumn? *Front Neuroanat* 2017; 11:116.
- Ossenkoppele, R., Cohn-Sheehy, B. I., La Joie, R., Vogel, J. W., Moller, C., Lehmann, M., van Berckel, B. N., Seeley, W. W., Pijnenburg, Y. A., Gorno-Tempini, M. L., Kramer, J. H., Barkhof, F., Rosen, H. J., van der Flier, W. M., Jagust, W. J., Miller, B. L., Scheltens, P.

- and Rabinovici, G. D. Atrophy patterns in early clinical stages across distinct phenotypes of Alzheimer's disease. *Human brain mapping* 2015a; 36:4421-37.
- Ossenkoppele, R., Pijnenburg, Y. A., Perry, D. C., Cohn-Sheehy, B. I., Scheltens, N. M., Vogel, J. W., Kramer, J. H., van der Vlies, A. E., La Joie, R., Rosen, H. J., van der Flier, W. M., Grinberg, L. T., Rozemuller, A. J., Huang, E. J., van Berckel, B. N., Miller, B. L., Barkhof, F., Jagust, W. J., Scheltens, P., Seeley, W. W. and Rabinovici, G. D. The behavioural/dysexecutive variant of Alzheimer's disease: clinical, neuroimaging and pathological features. *Brain : a journal of neurology* 2015b; 138:2732-49.
- Ossenkoppele, R., Schonhaut, D. R., Scholl, M., Lockhart, S. N., Ayakta, N., Baker, S. L., O'Neil, J. P., Janabi, M., Lazaris, A., Cantwell, A., Vogel, J., Santos, M., Miller, Z. A., Bettcher, B. M., Vessel, K. A., Kramer, J. H., Gorno-Tempini, M. L., Miller, B. L., Jagust, W. J. and Rabinovici, G. D. Tau PET patterns mirror clinical and neuroanatomical variability in Alzheimer's disease. *Brain : a journal of neurology* 2016; 139:1551-67.
- Patterson, K., Nestor, P. J. and Rogers, T. T. Where do you know what you know? The representation of semantic knowledge in the human brain. *Nature reviews. Neuroscience* 2007; 8:976-87.
- Pauling, L. and Coryell, C. D. The Magnetic Properties and Structure of Hemoglobin, Oxyhemoglobin and Carbonmonoxyhemoglobin. *Proceedings of the National Academy of Sciences of the United States of America* 1936; 22:210-6.
- Phelps, M. E., Hoffman, E. J., Mullani, N. A. and Ter-Pogossian, M. M. Application of annihilation coincidence detection to transaxial reconstruction tomography. *Journal of nuclear medicine : official publication, Society of Nuclear Medicine* 1975; 16:210-24.
- Phillips, J. S., Das, S. R., McMillan, C. T., Irwin, D. J., Roll, E. E., Da Re, F., Nasrallah, I. M., Wolk, D. A. and Grossman, M. Tau PET imaging predicts cognition in atypical variants of Alzheimer's disease. *Human brain mapping* 2018; 39:691-708.
- Power, J. D., Barnes, K. A., Snyder, A. Z., Schlaggar, B. L. and Petersen, S. E. Spurious but systematic correlations in functional connectivity MRI networks arise from subject motion. *NeuroImage* 2012; 59:2142-54.
- Power, J. D., Mitra, A., Laumann, T. O., Snyder, A. Z., Schlaggar, B. L. and Petersen, S. E. Methods to detect, characterize, and remove motion artifact in resting state fMRI. *NeuroImage* 2014; 84:320-41.
- Press, G. A., Amaral, D. G. and Squire, L. R. Hippocampal abnormalities in amnesic patients revealed by high-resolution magnetic resonance imaging. *Nature* 1989; 341:54-7.

- Rabin, L. A., Barr, W. B. and Burton, L. A. Assessment practices of clinical neuropsychologists in the United States and Canada: a survey of INS, NAN, and APA Division 40 members. *Arch Clin Neuropsychol* 2005; 20:33-65.
- Rabinovici, G. D., Carrillo, M. C., Forman, M., DeSanti, S., Miller, D. S., Kozauer, N., Petersen, R. C., Randolph, C., Knopman, D. S., Smith, E. E., Isaac, M., Mattsson, N., Bain, L. J., Hendrix, J. A. and Sims, J. R. Multiple comorbid neuropathologies in the setting of Alzheimer's disease neuropathology and implications for drug development. *Alzheimer's & dementia* 2017; 3:83-91.
- Raichle, M. E., Eichling, J. O., Straatmann, M. G., Welch, M. J., Larson, K. B. and Ter-Pogossian, M. M. Blood-brain barrier permeability of ^{11}C -labeled alcohols and ^{15}O -labeled water. *Am J Physiol* 1976; 230:543-52.
- Raichle, M. E., Larson, K. B., Phelps, M. E., Grubb, R. L., Jr., Welch, M. J. and Ter-Pogossian, M. M. In vivo measurement of brain glucose transport and metabolism employing glucose- ^{11}C . *Am J Physiol* 1975; 228:1936-48.
- Raichle, M. E., MacLeod, A. M., Snyder, A. Z., Powers, W. J., Gusnard, D. A. and Shulman, G. L. A default mode of brain function. *Proceedings of the National Academy of Sciences of the United States of America* 2001; 98:676-82.
- Resende, E. P. F., Nolan, A. L., Petersen, C., Ehrenberg, A. J., Spina, S., Allen, I. E., Rosen, H. J., Kramer, J., Miller, B. L., Seeley, W. W., Gorno-Tempini, M. L., Miller, Z. and Grinberg, L. T. Language and spatial dysfunction in Alzheimer disease with white matter thorn-shaped astrocytes: Astrocytic tau, cognitive function, and Alzheimer disease. *Neurology* 2020;
- Ridgway, G. R., Lehmann, M., Barnes, J., Rohrer, J. D., Warren, J. D., Crutch, S. J. and Fox, N. C. Early-onset Alzheimer disease clinical variants: multivariate analyses of cortical thickness. *Neurology* 2012; 79:80-4.
- Riedl, V., Bienkowska, K., Strobel, C., Tahmasian, M., Grimmer, T., Forster, S., Friston, K. J., Sorg, C. and Drzezga, A. Local activity determines functional connectivity in the resting human brain: a simultaneous FDG-PET/fMRI study. *The Journal of neuroscience : the official journal of the Society for Neuroscience* 2014; 34:6260-6.
- Roche, A., Meriaux, S., Keller, M. and Thirion, B. Mixed-effect statistics for group analysis in fMRI: a nonparametric maximum likelihood approach. *NeuroImage* 2007; 38:501-10.
- Rogalski, E., Cobia, D., Harrison, T. M., Wieneke, C., Thompson, C. K., Weintraub, S. and Mesulam, M. M. Anatomy of language impairments in primary progressive aphasia. *The*

Journal of neuroscience : the official journal of the Society for Neuroscience 2011a; 31:3344-50.

Rogalski, E., Cobia, D., Harrison, T. M., Wieneke, C., Weintraub, S. and Mesulam, M. M. Progression of language decline and cortical atrophy in subtypes of primary progressive aphasia. *Neurology* 2011b; 76:1804-10.

Rogalski, E., Cobia, D., Mardersteck, A., Rademaker, A., Wieneke, C., Weintraub, S. and Mesulam, M. M. Asymmetry of cortical decline in subtypes of primary progressive aphasia. *Neurology* 2014; 83:1184-91.

Rogalski, E., Johnson, N., Weintraub, S. and Mesulam, M. Increased frequency of learning disability in patients with primary progressive aphasia and their first-degree relatives. *Archives of neurology* 2008; 65:244-8.

Rogalski, E., Sridhar, J., Rader, B., Mardersteck, A., Chen, K., Cobia, D., Thompson, C. K., Weintraub, S., Bigio, E. H. and Mesulam, M. M. Aphasic variant of Alzheimer disease: Clinical, anatomic, and genetic features. *Neurology* 2016; 87:1337-43.

Rogalski, E., Weintraub, S. and Mesulam, M. M. Are there susceptibility factors for primary progressive aphasia? *Brain and language* 2013; 127:135-8.

Rogalski, E. J., Sridhar, J., Mardersteck, A., Rader, B., Cobia, D., Arora, A. K., Fought, A. J., Bigio, E. H., Weintraub, S., Mesulam, M. M. and Rademaker, A. Clinical and cortical decline in the aphasic variant of Alzheimer's disease. *Alzheimer's & dementia : the journal of the Alzheimer's Association* 2019; 15:543-552.

Rohrer, J. D., Warren, J. D., Modat, M., Ridgway, G. R., Douiri, A., Rossor, M. N., Ourselin, S. and Fox, N. C. Patterns of cortical thinning in the language variants of frontotemporal lobar degeneration. *Neurology* 2009; 72:1562-9.

Rosen, H. J., Gorno-Tempini, M. L., Goldman, W. P., Perry, R. J., Schuff, N., Weiner, M., Feiwell, R., Kramer, J. H. and Miller, B. L. Patterns of brain atrophy in frontotemporal dementia and semantic dementia. *Neurology* 2002; 58:198-208.

Rousset, O. G., Ma, Y. and Evans, A. C. Correction for partial volume effects in PET: principle and validation. *Journal of nuclear medicine : official publication, Society of Nuclear Medicine* 1998a; 39:904-11.

- Rousset, O. G., Ma, Y. L., Wong, D. F. and Evans, A. C. Pixel- versus region-based partial volume correction in PET. *Quantitative Functional Brain Imaging with Positron Emission Tomography* 1998b; 67-75.
- Rowe, C. C., Pejoska, S., Mulligan, R. S., Jones, G., Chan, J. G., Svensson, S., Cselenyi, Z., Masters, C. L. and Villemagne, V. L. Head-to-head comparison of ¹¹C-PiB and ¹⁸F-AZD4694 (NAV4694) for beta-amyloid imaging in aging and dementia. *Journal of nuclear medicine : official publication, Society of Nuclear Medicine* 2013; 54:880-6.
- Rumelhart, D. and McClelland, J. *Parallel distributed processing: explorations in the microstructure of cognition, vol. 1: foundations*. Cambridge, MA, USA: MIT Press; 1986.
- Sabri, O., Sabbagh, M. N., Seibyl, J., Barthel, H., Akatsu, H., Ouchi, Y., Senda, K., Murayama, S., Ishii, K., Takao, M., Beach, T. G., Rowe, C. C., Leverenz, J. B., Ghetti, B., Ironside, J. W., Catafau, A. M., Stephens, A. W., Mueller, A., Koglin, N., Hoffmann, A., Roth, K., Reininger, C., Schulz-Schaeffer, W. J. and Florbetaben Phase 3 Study, G. Florbetaben PET imaging to detect amyloid beta plaques in Alzheimer's disease: phase 3 study. *Alzheimer's & dementia : the journal of the Alzheimer's Association* 2015; 11:964-74.
- Sattarivand, M., Kusano, M., Poon, I. and Caldwell, C. Symmetric geometric transfer matrix partial volume correction for PET imaging: principle, validation and robustness. *Physics in medicine and biology* 2012; 57:7101-16.
- Savio, A., Funger, S., Tahmasian, M., Rachakonda, S., Manoliu, A., Sorg, C., Grimmer, T., Calhoun, V., Drzezga, A., Riedl, V. and Yakushev, I. Resting-State Networks as Simultaneously Measured with Functional MRI and PET. *Journal of nuclear medicine : official publication, Society of Nuclear Medicine* 2017; 58:1314-1317.
- Scheltens, P., Leys, D., Barkhof, F., Huglo, D., Weinstein, H. C., Vermersch, P., Kuiper, M., Steinling, M., Wolters, E. C. and Valk, J. Atrophy of medial temporal lobes on MRI in "probable" Alzheimer's disease and normal ageing: diagnostic value and neuropsychological correlates. *Journal of neurology, neurosurgery, and psychiatry* 1992; 55:967-72.
- Seab, J. P., Jagust, W. J., Wong, S. T., Roos, M. S., Reed, B. R. and Budinger, T. F. Quantitative NMR measurements of hippocampal atrophy in Alzheimer's disease. *Magnetic resonance in medicine : official journal of the Society of Magnetic Resonance in Medicine / Society of Magnetic Resonance in Medicine* 1988; 8:200-8.
- Seeley, W. W., Crawford, R. K., Zhou, J., Miller, B. L. and Greicius, M. D. Neurodegenerative diseases target large-scale human brain networks. *Neuron* 2009; 62:42-52.

- Segonne, F., Pacheco, J. and Fischl, B. Geometrically accurate topology-correction of cortical surfaces using nonseparating loops. *IEEE transactions on medical imaging* 2007; 26:518-29.
- Seo, S. W., Ayakta, N., Grinberg, L. T., Villeneuve, S., Lehmann, M., Reed, B., DeCarli, C., Miller, B. L., Rosen, H. J., Boxer, A. L., O'Neil, J. P., Jin, L. W., Seeley, W. W., Jagust, W. J. and Rabinovici, G. D. Regional correlations between [(11)C]PIB PET and post-mortem burden of amyloid-beta pathology in a diverse neuropathological cohort. *NeuroImage. Clinical* 2017; 13:130-137.
- Smith, S. M., Fox, P. T., Miller, K. L., Glahn, D. C., Fox, P. M., Mackay, C. E., Filippini, N., Watkins, K. E., Toro, R., Laird, A. R. and Beckmann, C. F. Correspondence of the brain's functional architecture during activation and rest. *Proceedings of the National Academy of Sciences of the United States of America* 2009; 106:13040-5.
- Sperling, R. A., Rentz, D. M., Johnson, K. A., Karlawish, J., Donohue, M., Salmon, D. P. and Aisen, P. The A4 study: stopping AD before symptoms begin? *Sci Transl Med* 2014; 6:228fs13.
- Strauss, E., Sherman, E. M. S., Spreen, O. and Spreen, O. A compendium of neuropsychological tests : administration, norms, and commentary. 3rd ed. Oxford ; New York: Oxford University Press; 2006.
- Sweeney, M. D., Montagne, A., Sagare, A. P., Nation, D. A., Schneider, L. S., Chui, H. C., Harrington, M. G., Pa, J., Law, M., Wang, D. J. J., Jacobs, R. E., Doubal, F. N., Ramirez, J., Black, S. E., Nedergaard, M., Benveniste, H., Dichgans, M., Iadecola, C., Love, S., Bath, P. M., Markus, H. S., Salman, R. A., Allan, S. M., Quinn, T. J., Kalaria, R. N., Werring, D. J., Carare, R. O., Touyz, R. M., Williams, S. C. R., Moskowitz, M. A., Katusic, Z. S., Lutz, S. E., Lazarov, O., Minshall, R. D., Rehman, J., Davis, T. P., Wellington, C. L., Gonzalez, H. M., Yuan, C., Lockhart, S. N., Hughes, T. M., Chen, C. L. H., Sachdev, P., O'Brien, J. T., Skoog, I., Pantoni, L., Gustafson, D. R., Biessels, G. J., Wallin, A., Smith, E. E., Mok, V., Wong, A., Passmore, P., Barkof, F., Muller, M., Breteler, M. M. B., Roman, G. C., Hamel, E., Seshadri, S., Gottesman, R. F., van Buchem, M. A., Arvanitakis, Z., Schneider, J. A., Drewes, L. R., Hachinski, V., Finch, C. E., Toga, A. W., Wardlaw, J. M. and Zlokovic, B. V. Vascular dysfunction-The disregarded partner of Alzheimer's disease. *Alzheimer's & dementia : the journal of the Alzheimer's Association* 2019; 15:158-167.
- Ter-Pogossian, M. M., Eichling, J. O., Davis, D. O., Welch, M. J. and Metzger, J. M. The determination of regional cerebral blood flow by means of water labeled with radioactive oxygen 15. *Radiology* 1969; 93:31-40.

- Ter-Pogossian, M. M., Phelps, M. E., Hoffman, E. J. and Mullani, N. A. A positron-emission transaxial tomograph for nuclear imaging (PETT). *Radiology* 1975; 114:89-98.
- Tisdall, M. D., Hess, A. T., Reuter, M., Meintjes, E. M., Fischl, B. and van der Kouwe, A. J. Volumetric navigators for prospective motion correction and selective reacquisition in neuroanatomical MRI. *Magnetic resonance in medicine : official journal of the Society of Magnetic Resonance in Medicine / Society of Magnetic Resonance in Medicine* 2012; 68:389-99.
- van den Heuvel, M. P. and Sporns, O. A cross-disorder connectome landscape of brain dysconnectivity. *Nature reviews. Neuroscience* 2019; 20:435-446.
- van Sluis, J., de Jong, J., Schaar, J., Noordzij, W., van Snick, P., Dierckx, R., Borra, R., Willemsen, A. and Boellaard, R. Performance Characteristics of the Digital Biograph Vision PET/CT System. *Journal of nuclear medicine : official publication, Society of Nuclear Medicine* 2019; 60:1031-1036.
- Vandenberghe, R., Van Laere, K., Ivanoiu, A., Salmon, E., Bastin, C., Triau, E., Hasselbalch, S., Law, I., Andersen, A., Korner, A., Minthon, L., Garraux, G., Nelissen, N., Bormans, G., Buckley, C., Owenius, R., Thurfjell, L., Farrar, G. and Brooks, D. J. 18F-flutemetamol amyloid imaging in Alzheimer disease and mild cognitive impairment: a phase 2 trial. *Annals of neurology* 2010; 68:319-29.
- Villemagne, V. L., Ong, K., Mulligan, R. S., Holl, G., Pejoska, S., Jones, G., O'Keefe, G., Ackerman, U., Tochon-Danguy, H., Chan, J. G., Reiningner, C. B., Fels, L., Putz, B., Rohde, B., Masters, C. L. and Rowe, C. C. Amyloid imaging with (18)F-florbetaben in Alzheimer disease and other dementias. *Journal of nuclear medicine : official publication, Society of Nuclear Medicine* 2011; 52:1210-7.
- Wang, L., Benzinger, T. L., Su, Y., Christensen, J., Friedrichsen, K., Aldea, P., McConathy, J., Cairns, N. J., Fagan, A. M., Morris, J. C. and Ances, B. M. Evaluation of Tau Imaging in Staging Alzheimer Disease and Revealing Interactions Between beta-Amyloid and Tauopathy. *JAMA neurology* 2016; 73:1070-7.
- Weintraub, S., Mesulam, M. M., Wieneke, C., Rademaker, A., Rogalski, E. J. and Thompson, C. K. The northwestern anagram test: measuring sentence production in primary progressive aphasia. *American journal of Alzheimer's disease and other dementias* 2009; 24:408-16.
- Whitwell, J. L., Jones, D. T., Duffy, J. R., Strand, E. A., Machulda, M. M., Przybelski, S. A., Vemuri, P., Gregg, B. E., Gunter, J. L., Senjem, M. L., Petersen, R. C., Jack, C. R., Jr. and Josephs, K. A. Working memory and language network dysfunctions in logopenic

- aphasia: a task-free fMRI comparison with Alzheimer's dementia. *Neurobiology of aging* 2014;
- Win, K. T., Pluta, J., Yushkevich, P., Irwin, D. J., McMillan, C. T., Rascovsky, K., Wolk, D. and Grossman, M. Neural Correlates of Verbal Episodic Memory and Lexical Retrieval in Logopenic Variant Primary Progressive Aphasia. *Frontiers in neuroscience* 2017; 11:330.
- Winkler, A. M., Ridgway, G. R., Webster, M. A., Smith, S. M. and Nichols, T. E. Permutation inference for the general linear model. *NeuroImage* 2014; 92:381-97.
- Wong, D. F., Rosenberg, P. B., Zhou, Y., Kumar, A., Raymond, V., Ravert, H. T., Dannals, R. F., Nandi, A., Brasic, J. R., Ye, W., Hilton, J., Lyketsos, C., Kung, H. F., Joshi, A. D., Skovronsky, D. M. and Pontecorvo, M. J. In vivo imaging of amyloid deposition in Alzheimer disease using the radioligand 18F-AV-45 (florbetapir [corrected] F 18). *Journal of nuclear medicine : official publication, Society of Nuclear Medicine* 2010; 51:913-20.
- Xia, C., Makaretz, S. J., Caso, C., McGinnis, S., Gomperts, S. N., Sepulcre, J., Gomez-Isla, T., Hyman, B. T., Schultz, A., Vasdev, N., Johnson, K. A. and Dickerson, B. C. Association of In Vivo [18F]AV-1451 Tau PET Imaging Results With Cortical Atrophy and Symptoms in Typical and Atypical Alzheimer Disease. *JAMA neurology* 2017; 74:427-436.
- Xia, C. F., Arteaga, J., Chen, G., Gangadharmath, U., Gomez, L. F., Kasi, D., Lam, C., Liang, Q., Liu, C., Mocharla, V. P., Mu, F., Sinha, A., Su, H., Szardenings, A. K., Walsh, J. C., Wang, E., Yu, C., Zhang, W., Zhao, T. and Kolb, H. C. [(18)F]T807, a novel tau positron emission tomography imaging agent for Alzheimer's disease. *Alzheimer's & dementia : the journal of the Alzheimer's Association* 2013; 9:666-76.
- Yeo, B. T., Krienen, F. M., Eickhoff, S. B., Yaakub, S. N., Fox, P. T., Buckner, R. L., Asplund, C. L. and Chee, M. W. Functional Specialization and Flexibility in Human Association Cortex. *Cerebral cortex* 2014;
- Yeo, B. T., Krienen, F. M., Sepulcre, J., Sabuncu, M. R., Lashkari, D., Hollinshead, M., Roffman, J. L., Smoller, J. W., Zollei, L., Polimeni, J. R., Fischl, B., Liu, H. and Buckner, R. L. The organization of the human cerebral cortex estimated by intrinsic functional connectivity. *Journal of neurophysiology* 2011; 106:1125-65.